Mathematical Modelling of a Novel Hetero-junction SIS Front Surface and Interdigitated Back Contact Solar Cell

Kaustuv Dasgupta (kaustuvdasgupta83@gmail.com)
Meghnad Saha Institute of Technology https://orcid.org/0000-0003-1819-4627
Anup Mondal
IIEST Shibpur: Indian Institute of Engineering Science and Technology
Soma Ray
IIEST Shibpur: Indian Institute of Engineering Science and Technology
Utpal Gangopadhyay
Meghnad Saha Institute of Technology

Research Article

Keywords: Interdigitated back contact solar cell, SIS solar cell, MATLAB, ZnO, Mathematical modelling

Posted Date: April 12th, 2021

DOI: https://doi.org/10.21203/rs.3.rs-389030/v1

Version of Record: A version of this preprint was published at Journal of Computational Electronics on August 22nd, 2021. See the published version at https://doi.org/10.1007/s10825-021-01735-2.

Mathematical Modelling of a Novel Hetero-junction SIS front surface and interdigitated back contact Solar Cell

Kaustuv Dasgupta[*a,b], Anup Mondal[c], Soma Ray[a,b], Utpal Gangopadhyay[a]

[a]*Centre for Advance Research in Renewable Energy and Sensor Technology,Meghnad Saha institute of Technology, Kolkata-700150, India*
[b]*Centre for Green Energy and Sensor System, IIEST, Howrah-711103, India*
[c]*Department ofChemistry, IIEST, Howrah-711103, India*

*Correspondence to kaustuvdasgupta83@gmail.com

Key words: **Interdigitated back contact solar cell, SIS solar cell, MATLAB, ZnO, Mathematical modelling**

Abstract

In this paper we have proposed the design and fabrication of a novel hetero junction SIS front surface and interdigitated back contact solar cell. We have approximated the performance parameters and loss analysis of the proposed solar cell by using MATLAB software programming. Many groups of scientists have reported the experimental analysis of a-Si back contact interdigitated solar cell in different studies. Many silicon hetero junction solar cell design and results have been reported with some promising efficiency in last few decades. In this study a high life time(~2 ms) n-Si substrate was considered so that a sufficient amount of light generated career can reach to the interdigitated layer to get absorbed. The availability of the careers at the interdigitated back surface was further enhanced by considering and high-low junction at the front surface created by a ZnO n^+ layer at the front surface. A very thin layer of thermally generated insulator SiO_2 was considered in between ZnO and n-Si. This layer improves the detrimental effect of interface defects. This is the first time we have theorized interdigitated back contact (IBC) solar cell using metal oxide semiconductors layer deposition avoiding the expensive and complicated doping and diffusion process. In general a high concentration n^+ layer is doped to create the high-low junction at front to accelerate the carriers to the back junctions. We are proposing a cost effective thermal deposition of SiO_2 layer followed by sol-gel ZnO layer deposition which serves the same purpose of an n^+ layer by introducing an SIS junction potential at front. The interdigitated back surface was designed with subsequent n^+ a:Si and p^+ a:Si vertical junctions.

1. Introduction

The optimization of front surface metallisation has always been a challenge for designing of solar cell. In one hand, less metallic contact on the front surface increases the front surface layer resistivity causing a high internal series resistance of the solar cell. High series resistance is a constraint to achieve higher efficiency. On the other hand, we can decrease the series resistance using different grid pattern of closely placed metal contact but that causes greater shading effect. Light getting into the cell is reduced resulting lower efficiency. To resolve this dilemma Schwartz et al designed and fabricated a solar cell in 1975 [1]. They reported a solar cell which had all the metal contact on the back surface. The back surface was fabricated with sequential n^+ and p^+ layers parallel to the rays of light falling on the cell. This interdigitated back surface creates multiple junctions at the back. The open circuit voltage arises from junction built in potentials as per connection. The short circuit current of IBC solar cell largely depends on the bulk lifetime [2]. The carrier transportation can be modified by creating a front surface field (FSF). This FSF enhance the photo generated current at the back surface interdigitated junctions. Recently Bao et al has reported a theoretical analysis to show the effect of FSF created by a-Si:H n^+ layer upon c-Si n substrate [3]. In this paper we have adopted a different approach to analyse the overall performance of c-Si n substrate based a-Si:H n^+ and a-Si:H p^+ IBC solar cell with and without FSF. We have investigated the effect of FSF formed by an SIS Schottkey junction (FSF1). We have presented a comparative performance analysis between the effect of FSF1 and FSF2 (created by n+ amorphous front layer) on IBC without solar FSF.

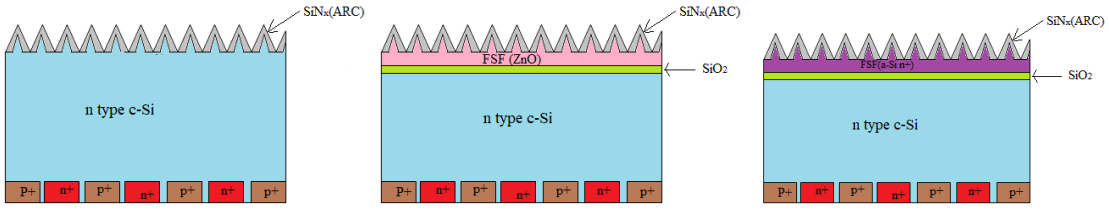

Fig. 1a -1c Structure of interdigitated back contact solar cell with and without FSF

A suitable mathematical model for the Interdigitated Back Contact (IBC) solar cell, as depicted in Fig. 1a -1c, has been presented with help of MATLAB programming. First the simple IBC structure without BSF (Fig. 1a) is theorized by solving second order transport equation and corresponding energy band diagram. Then the same was followed for IBC with BSF (n+ ZnO) structure as shown in Fig. 1b. Fig. 1c is shown to describe our novel IBC structure with schottkey hetero junction SIS FSF (n+ a Si). Further the effect of BCI finger width was studied on solar cell performance. Finger width optimization has always been a important factor to IBC solar cell performance [4-5]. We have tried to find an amicable solution to optimize the finger width in this mathematical modelling. In this study an n type c-Si with high lifetime substrate was considered. The front surface was considered passivated with anti reflection coating (ARC) of SiN_X layer. The back surface IBC was designed with subsequent n^+ and p^+ a-Si:H fingers. n^+ finger acts as emitter while p^+ fingers provides back surface field (BSF). Further the IBC cell was modified by a tunnelling SiO_2 layer and ZnO layer (deposited by sol-gel method) to form an FSF. All the physical properties and structure parameters are considered as reported elsewhere are listed in the following Table 1.

Table 1 Material properties and structure parameters considered in the mathematical modelling (at 300K)

Material	Dimensions	Properties
ARC(SiN_x)	Thickness d_{ARC} = 75nm [6]	refractive index n=2.05[6]
FSF2 (n-type ZnO)	Thickness d_{FSF} = 400 nm [7]	carrier concentration $N_{DZnO} = 8 \times 10^{18}$ cm^{-3} [7] Energy band gap E_{gZnO} = 3.37 eV [8] Electron affinity χ_{ZnO} = 4.5eV [8] Effective mass of electron $m_{nZnO}^* = 0.24\ m_0$ [9] Effective mass of hole $m_{pZnO}^* = 0.59 m_0$ [9] Relative permittivity ε_{ZnO} = 8.5[10]
Tunnelling insulator (SiO_2)	Thickness d_{sio2} = 5 nm [11]	
Emitter finger (a-Si:H p^+)	width W_{BSF} = 500 µm [2] Thickness d_{BSF} = 10 µm	carrier concentration $N_{AaSi} = 8 \times 10^{18}$ cm^{-3} [12] Energy band gap E_{gaSi} = 1.7 eV[3] Electron affinity χ_{aSi} = 3.8 eV [3] Effective density of state conduction band edge $N_{CaSi} = 4.5 \times 10^{21}$ cm^{-3} [13] Effective density of state valance band edge $N_{VaSi} = 6.4 \times 10^{21}$ cm^{-3} [13] Drift mobility of electron μ_{naSi} = 1 cm^2/Vs [13] Drift mobility of hole μ_{paSi} = 0.01 cm^2/Vs [13] electron lifetime τ_{naSi} = 900µs [14] Back surface recombination velocity S_{BSF} = 10 cm/s [15]
BSF finger (a-Si:H n^+)/FSF2	width $W_{emitter}$ = 150 µm [2] Thickness $d_{emitter}$ = 6 µm	carrier concentration $N_{DaSi} = 5 \times 10^{19}$ cm^{-3} [12] Energy band gap E_{gaSi} = 1.72 eV [3] Electron affinity χ_{aSi} = 3.7 eV [3] Relative permittivity ε_{cSi} = 6[12] Effective density of state conduction band edge $N_{CaSi} = 4.5 \times 10^{21}$ cm^{-3} [13] Effective density of state valance band edge $N_{VaSi} = 6.4 \times 10^{21}$ cm^{-3} [13] Drift mobility of electron μ_{naSi} = 1 cm^2/Vs [13] Drift mobility of hole μ_{paSi} = 0.01 cm^2/Vs [13] hole lifetime τ_{paSi} = 700µs [14] Back surface recombination velocity $S_{emitter}$ = 10 cm/s [15]
c-Si n-type substrate (bulk)	Thickness d_{bulk} = 300 µm [6]	carrier concentration $N_{DcSi} = 2 \times 10^{16}$ cm^{-3} [12] Energy band gap E_{gcSi} = 1.12 eV [13] Electron affinity χ_{cSi} = 4.05 eV [13] Relative permittivity ε_{cSi} = 11.9[13] Effective density of state conduction band edge $N_{CcSi} = 2.82 \times 10^{19}$ cm^{-3} [13] Effective density of state valance band edge $N_{VcSi} = 1.83 \times 10^{19}$ cm^{-3} [13] Drift mobility of electron μ_{ncSi} = 1400 cm^2/Vs [13] Drift mobility of hole μ_{pcSi} = 480 cm^2/Vs [13] Best carrier lifetime τ_{bulk} = 2000µs [14]
Overall IBC solar cell	Area = 1 cm^2 Font surface texture pyramid height = 3 µm [5]	Front surface recombination velocity (FSRV) S_F = 500 cm/s [6] Back surface recombination velocity (BSRV)

		S_B = 500 cm/s [6] contact resistance 0.1 Ω/cm^2 [3]

Here we have considered some ideal conditions which have negligible effects on the actual values. These are listed below.

1. Surface recombination and the fringe effect at the edge are neglected. [4][16]

2. The ideality factor of each p-n junction is considered to be one. [16]

3. The cell parameters are considered to be two dimensional homogeneous, that is the 2D cell unit structure shown is the Fig. 2 is considered to be repeated along horizontal axis throughout the cell.

4. The FSF is considered to have no effect on dark saturation current. There are no electrodes at the front surface.

5. Photo generation of carrier at FSF layer was considered to be negligible with respect to the bulk layer generation.

6. The effect of FSF layer was only considered at bulk region.

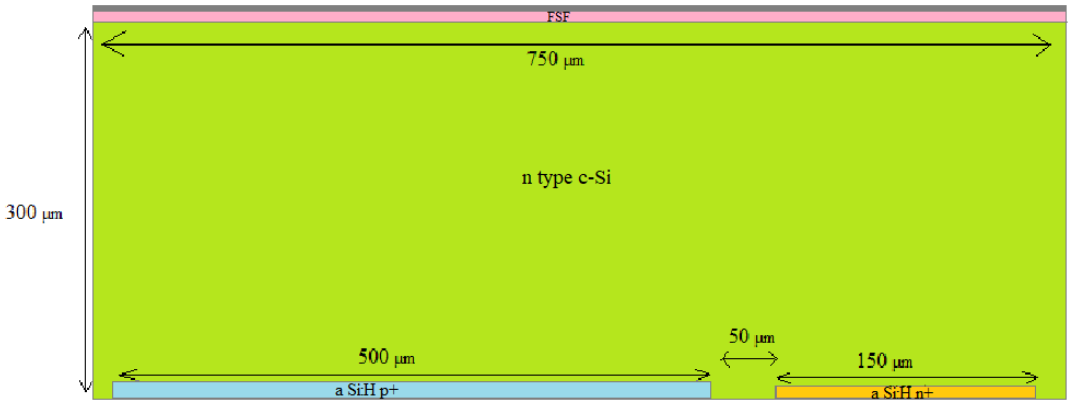

Fig. 2 Unit Cell Structure

Fig. 2 is showing the unit cell structure of IBC solar cell. This structure is considered as the basic unit. If the total width of the cell is of W μm. Then there are W/750 numbers of such units exists in the cell. In this study we have considered three cases for FSF.

Case I : No FSF is considered.

Case II : FSF formed by ZnO-SiO_2-C-Si(n type) SIS junction

Case III : : FSF formed by a-Si:H n^+- C-Si(n type) hetero junction.

We have simulated the above cases with MATLAB software and made a comparative analysis. We have solved basic partial differential equations (PDE) to get the values of collection probability and generated photo carriers at each point of the 2D model of the cell as shown in Fig. 2. Hence we have evaluated the photo generated current integrating all the values. The dark saturation current is a junction property. We have calculated dark current from the appropriate band diagram of IBC hetero junction. The front junction plays no role in photo collection and hence dark current density does not depend up on the nature of FSF.

2. Energy band diagram and dark saturation current

The interdigitated back contact is formed by a-Si:H n^+- C-Si(p type) - a-Si:H p^+ hetero junction. The energy band diagram of this hetero junction device is shown in Fig. 3.The built in potential was estimated from the band bending of the hetero junction. When the device reaches its equilibrium the Fermi level throughout the device must be constant.

The built in potential of the a-Si:H n^+- C-Si(p type) junction and C-Si(p type) - a-Si:H p^+ junction contribute to the overall built in potential of the device. Analytically if the built in potential ψ_1 arises from band bending of junction 1 ($E_1 - E_2$) and ψ_2 from band bending of junction 2 ($E_2 - E_3$) then the total built in potential $\psi = \psi_1 + \psi_2$ is due to total band bending $(E_1 - E_2) - (E_2 - E_3) = (E_1 - E_3)$. This implies that the overall built in potential can be estimated from equivalent band bending of junction between a-Si:H n^+ and a-Si:H p^+ minus ΔE_g. Where ΔE_g is the difference between bandgap energy of amorphous silicon and crystalline silicon. We have estimated the value of resultant built in potential by equivalent homo-junction of amorphous silicon. We have applied the Fermi-Dirac statistical distribution to get the junction built in potential [17].

$$\Psi = \frac{1}{q}\left[k_B T \ln\left(\frac{N_{AaSi} N_{DaSi}}{n_{iaSi}^2} \right) - \left(E_{gaSi} - E_{gcSi} \right) \right] \text{.....(1)}$$

where n_{iaSiH} is the intrinsic concentration of amorphous hydrogenated silicon which can be derived from the equation as described by Markvart et al [18].

$$n_{iaSi} = \left(N_{CaSi} N_{VaSi} \right)^{1/2} \exp(-E_{gaSi} / 2k_B T) \text{.....(2)}$$

Further the dark saturation current density was computed as a function of built in potential.

$$J_0 = q e^{-q\psi / k_B T} \left[N_{AaSi} \sqrt{\frac{D_{paSi}}{\tau_{paSi}}} + N_{DaSi} \sqrt{\frac{D_{naSi}}{\tau_{naSi}}} \right] \text{.....(3)}$$

The diffusion coefficient was calculated from Einstein's equation

$$D = \frac{kT}{q} \mu \text{.....(4)}$$

3. Collection probability and photo-generated current

The well accepted photo-generated current density equation is written for the two dimensional unit cell structure as shown in Fig. 2.

$$J_L^{'} = \int_{x=0}^{300\mu m} \int_{y=0}^{750\mu m} \int_{\lambda=280nm}^{1100nm} C_P(x,y) \left(H_0 \alpha(\lambda)(\lambda) e^{(-\alpha x)} \left(1 - R(\lambda) \right) d\lambda \right) dx dy \text{.....(5)}$$

If the width of the unit cell structure is w cm (0.075 cm) then the photo generated current density in A/cm^2 is expressed by following equation.

$$J_L = J_L^{'} / w \text{ A/cm}^2 \text{.....(6)}$$

First we have calculated the generated carrier distribution throughout the unit cell structure using photon flux data of standard AM 1.5 irradiance data. The front surface texturization is considered as micro-pyramidal texture of 3μm to 5μm created by conventional KOH-IPA alkaline etching method. The R(λ) data is extracted from the experimental graph of such texturization [19]. The absorption coefficient value of Si was taken from data published by Green et al [20]. Since we have neglected the photo generation at FSF in our mathematical model the photo generated carrier distribution was unchanged for all the cases that we have considered.

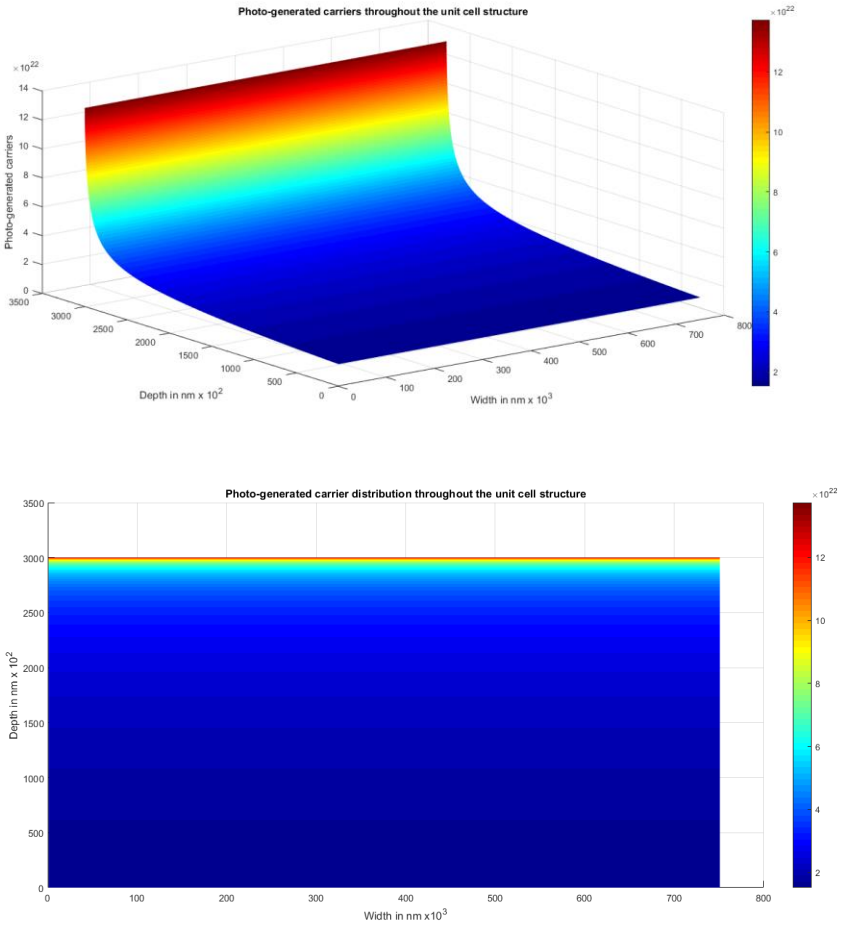

Fig. 3a-3b Photo-generated carrier distribution throughout unit cell structure

We have shown the generated photo carriers throughout the unit cell structure for total spectra of AM 1.5 irradiance in Fig. 3a-3b. Now the challenge was to get the collection probability throughout the unit cell structure. The collection probability largely depends upon surface recombination and minority carrier lifetime. We have considered three cases with different FSF and analysed the effect of it in collection probability. The insightful invention of Donolato was used to estimate the collection probability of the photo-generated carriers shown in Fig. 3a-3b. In 1985 Donolato proposed the reciprocity theorem, which stated as "The current collected by p-n junction as a unit carrier point charge is generated at a point P(x)(where x is the distance of point P from surface) is quantitively same as excess minority charge density at point P(x) due to unit density of carrier at the p-n junction edge"[21]. Later in 1994 the theorem was formulated for two dimensional application [22]. Two dimensional partial differential equation for collection probability ($C_P(x,y)$) was found out as,

$$D\left(\frac{\partial^2 C_P(x,y)}{\partial x^2}+\frac{\partial^2 C_P(x,y)}{\partial y^2}\right)-\frac{1}{\tau}C_P(x,y)=0.....(7)$$

Where D is the coefficient of diffusion and τ is the life time of minority carriers.

We have considered the boundaries of unit cell structure in which photo- carriers are generated. Different boundary conditions were considered to solve equation 7 for these three different regions.

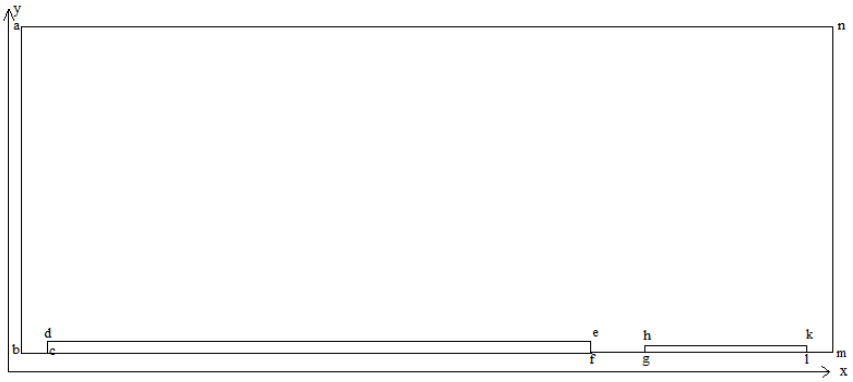

Fig. 4 Boundaries of unit cell structure

The bulk region boundaries are shown in Fig. 4. While determining the boundary conditions we have followed two fundamental considerations. First, the collection probability at junction edge is always unity. All the carriers generated at the junction edge were immediately collected. Second, the boundary conditions for boundaries which define the surface of the cell were set as Neumann condition determined by the surface recombination velocity. The different boundary conditions are explained below,

a→b and m→n : Neumann condition

$$-\frac{\partial C_P(x,y)}{\partial n_f}=0 \text{.....(8)}$$

As per our assumption the recombination velocity at the edge was zero.

b→c, f→g and l→m : Neumann condition

$$-\frac{\partial C_P(x,y)}{\partial n_f}=\left(S_B \big/ D_{pcSi}\right) C_P(x,y) \text{.....(9)}$$

S_B was the back surface recombination velocity for c-Si.

n→a: Neumann condition

$$-\frac{\partial C_P(x,y)}{\partial n_f}=\left(S_F \big/ D_{pcSi}\right) C_P(x,y) \text{.....(10)}$$

S_F was the front surface recombination velocity for c-Si.

c→d, d→e and e→f : these are junction boundaries. We have considered the Dirichlet condition.

$$C_P(x,y)=1 \text{.....(11)}$$

c→f : Neumann condition

$$-\frac{\partial C_P(x,y)}{\partial n_f}=\left(S_{BSF} \big/ D_{na\mathrm{Si}}\right) C_P(x,y) \text{.....(12)}$$

S_{BSF} was the surface recombination velocity of the BSF back surface.

g→l : Neumann condition

$$-\frac{\partial C_P(x,y)}{\partial n_f} = \left(S_{emitter} / D_{paSi} \right) C_P(x,y) \text{.....(13)}$$

$S_{emitter}$ was the surface recombination velocity of the emitter back surface.

We have solved reciprocity theorem equation 7 considering the boundary conditions (equation 8-11) for three different cases of three different FSF materials.

Case I : No FSF was considered.

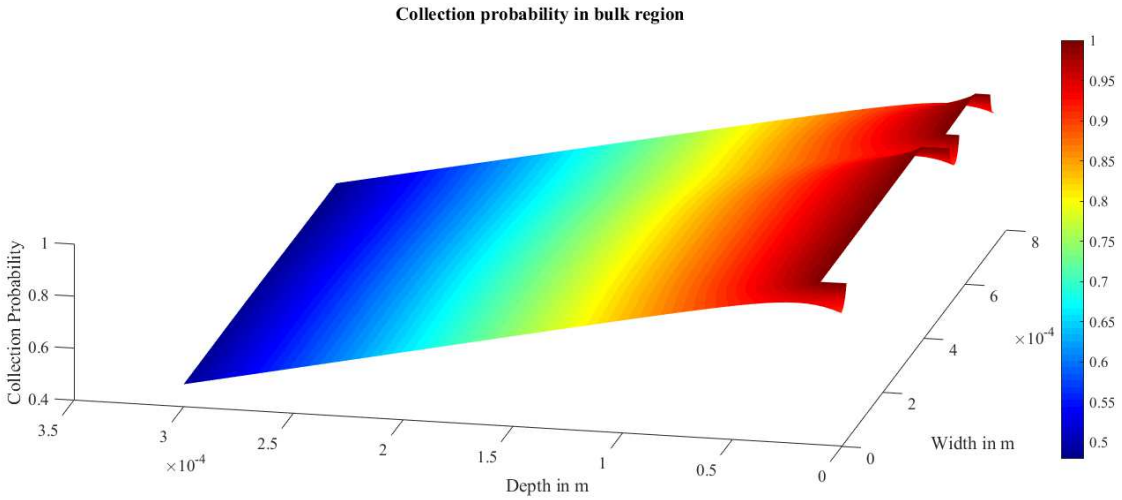

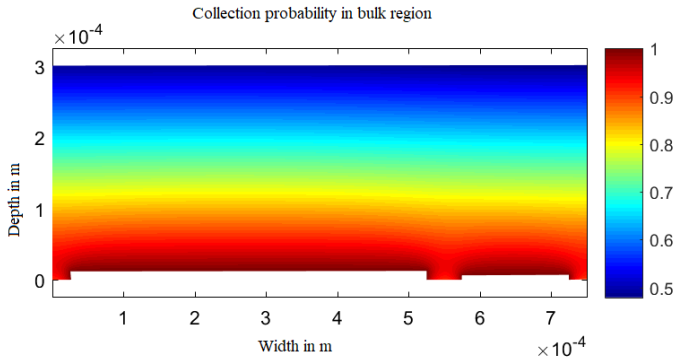

Fig. 5a-5b Collection probability profile in bulk region for Case I

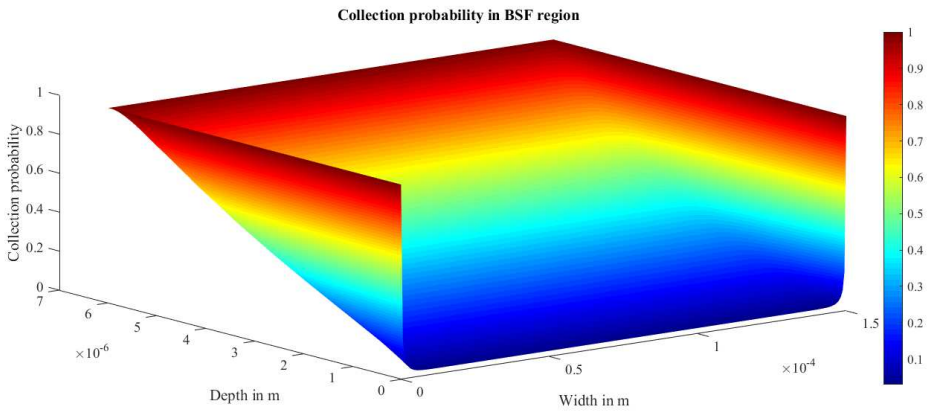

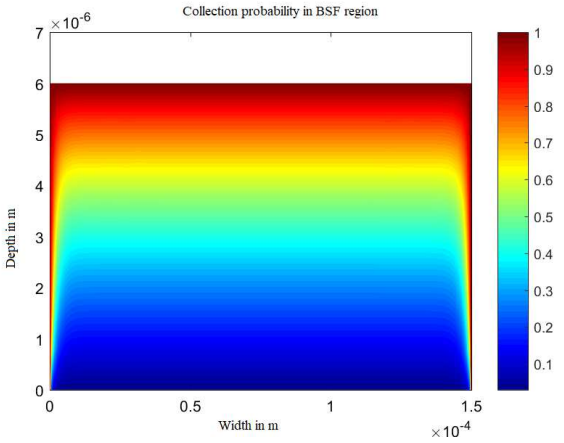

Fig. 6a-6b Collection probability profile in emitter region

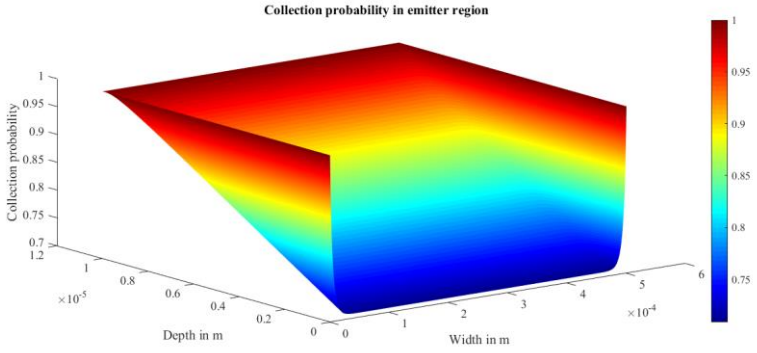

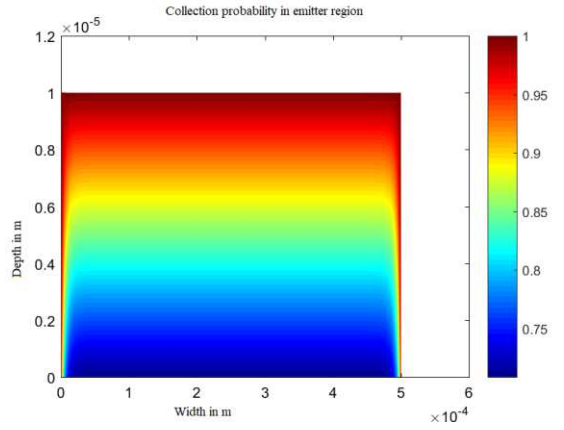

Fig. 7a-7b Collection probability profile in emitter region

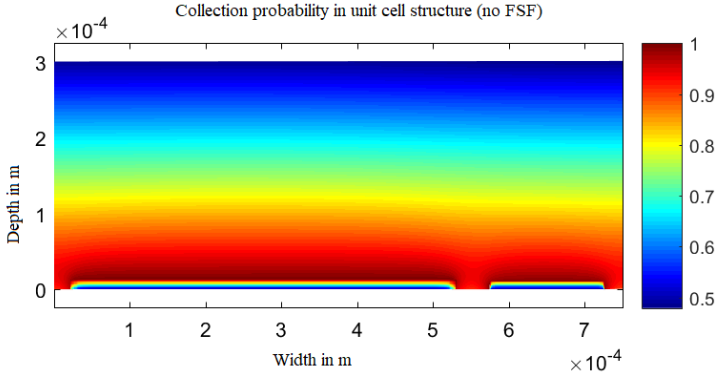

Fig. 8 Collection probability profile in entire unit cell structure for Case I

We have got Fig 5a-5b, Fig. 6a-6b and Fig. 7a-7b by solving the PDE in MATLAB. The collection probability profile of bulk, BSF and emitter regions are shown respectively. The total collection probability $C_p(x,y)$ has been shown in Fig. 8. Theoretically the light generated current density for unit cell structure was computed by multiplying mesh point to mesh point values of Fig. 3b (photo-generated carriers) and Fig. 8 (collection probability). The Photo-generated current for unit cell structure hence calculated as

$$J_L^{'} = 2.329 \text{ mA}$$

Hence the light generated current density for the IBC was calculated as,

$$J_L = {}^{2.118}\!/_{0.075} = 28.24 \text{ mA/cm}^2$$

case II : FSF formed by ZnO-SiO_2-C-Si(n type) SIS junction

In Case II we have considered our novel proposition of FSF induced by the front surface SIS junction with n type ZnO layer. The material properties of ZnO were considered from different reports published earlier as listed in Table 1. The SIS junction energy band diagram was helpful to find the built in potential across FSF.

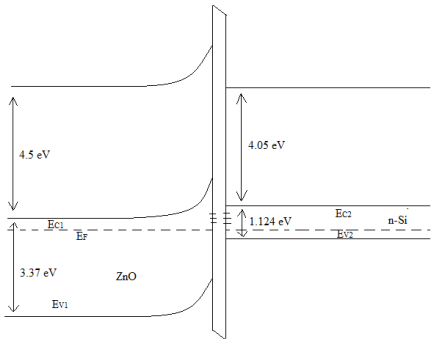

Fig. 9 Energy band diagram of FSF SIS junction

From the energy band bending as shown in Fig. 9 the potential was calculated [23].

$$\Psi_{FSF1} = \frac{1}{q}\left[\chi_{cSi} - \chi_{ZnO} + E_{gcSi} - k_B T \ln\left(\frac{N_{VcSi} N_{CZnO}}{N_{AcSi} N_{DZnO}}\right)\right] \text{.....(14)}$$

The field estimated from equation 13 accelerates the carriers to reach to the back surface junction and get collected. Thus the probability of a carrier to get collected is enhanced in presence of FSF. This effect was reflected in collection probability profile. We have used the continuity equation for electron to understand the effect of this FSF [24].

$$\frac{\partial \mathrm{V}p}{\partial t} = \mu_p \mathrm{V}p \frac{\partial E}{\partial y} + \mu_n E \frac{\partial \mathrm{V}p}{\partial y} + D_p \frac{\partial^2 \mathrm{V}p}{\partial y^2} + (G_p - R_p) \text{.....(15)}$$

In equation 14 E is the electric field in quasi neutral area. G_p and R_p are the generation and recombination rates. In Case I as there was no FSF the E was considered to be zero. Hence the continuity equation was reduced to equation 15.

$$\frac{\partial^2 \Delta p}{\partial y^2} = \frac{\Delta p}{D_p \tau_p} \text{.....(16)}$$

In presence of FSF there will be an electric field due to the built in potential at SIS junction as given by equation 13. Considering the steady state with no generation equation 14 can written as,

$$\mu_p \mathrm{V}p \frac{\partial E}{\partial y} + \mu_p E \frac{\partial \mathrm{V}p}{\partial y} + D_p \frac{\partial^2 \mathrm{V}p}{\partial y^2} = \frac{\mathrm{V}p}{\tau_p} \text{.....(17)}$$

Here the recombination rate is taken as,

$$R_p = \frac{\mathrm{V}p}{\tau_p} \text{.....(18)}$$

We noticed equation 15 and equation 17 mutually exclusive and do not satisfy equation 16. Hence we consider effective lifetime τ_{eff} in equation 17 for changed recombination rate in presence of FSF. Equation 16 was rewritten taking the values from equation 15.

$$\mu_p \mathrm{V}p \frac{\partial E}{\partial y} + \mu_p E \frac{\partial \mathrm{V}p}{\partial y} + \frac{\mathrm{V}p}{\tau_p} = \frac{\mathrm{V}p}{\tau_{eff}} \text{.....(19)}$$

Further considering no change in carrier concentration in bulk, the change in carrier lifetime was established as,

$$\frac{1}{\tau_p} - \frac{1}{\tau_{eff}} = \mu_p \frac{\partial^2 \psi_{FSF1}}{\partial y^2} \text{.....(20)}$$

From Poisson's equation at junction we found the derivative of built in potential.

$$\frac{\partial^2 \psi_{FSF1}}{\partial y^2} = \frac{q}{\varepsilon_0}\left(\frac{N_{DZnO}}{\varepsilon_{ZnO}} - \frac{N_{DcSi}}{\varepsilon_{cSi}}\right) \text{.....(21)}$$

Here we have considered the excess carrier concentration is considerably high and electric field is not changing only with respect to y axis (Fig. 4). We have then approximated the effective carrier lifetime from equation 19 and then solved the PDE of equation 7 using appropriate boundary condition of equation 8-11.

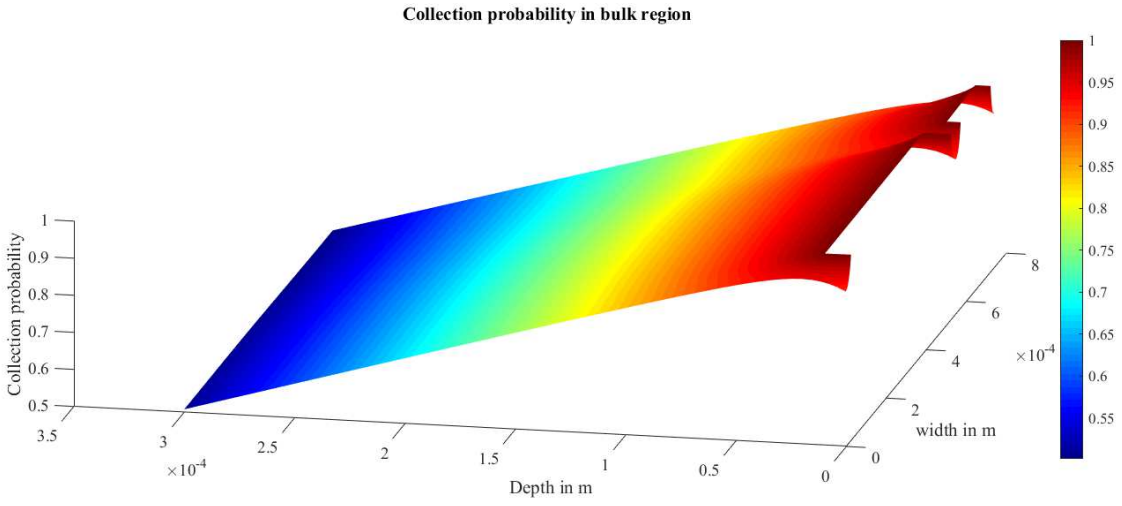

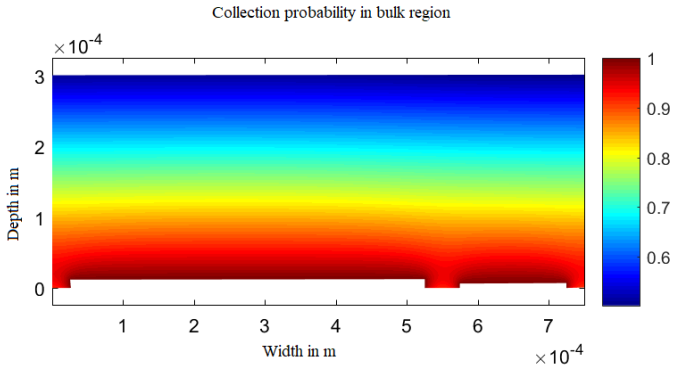

Fig. 10a-10b Collection probability profile in bulk region for Case II

Comparing Fig. 5a-5b with Fig. 10a-10b we concluded that there is a significant improvement in collection probability in bulk region. As per our assumption the collection probability profile in BSF and emitter region will be as same as case I.

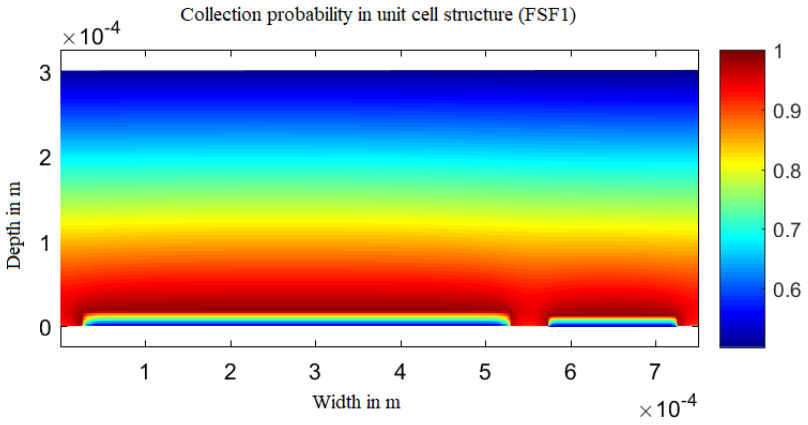

Fig. 11 Collection probability profile in entire unit cell structure for Case II

In Fig. 11 we have shown the total collection probability profile of unit cell structure. Following same method as case I we have got the light generated current density for case II as 32.67 mA/cm^2.

Case III : : FSF formed by a-Si:H n$^+$- C-Si(p type) hetero junction

We have followed the same approach to calculate the photo generated current in case III. The built in potential was found out from the following equation.

$$\Psi_{FSF2} = \frac{1}{q}\left[\chi_{cSi} - \chi_{aSi} + E_{gcSi} - k_B T \ln\left(\frac{N_{VcSi}N_{CaSi}}{N_{AcSi}N_{DaSi}}\right)\right] \text{.....(22)}$$

Effective life time was calculated likewise,

$$\frac{1}{\tau_p} - \frac{1}{\tau_{eff}^{'}} = \mu_p \frac{\partial^2 \psi_{FSF2}}{\partial y^2} \text{.....(23)}$$

And

$$\frac{\partial^2 \psi_{FSF2}}{\partial y^2} = \frac{q}{\varepsilon_0}\left(\frac{N_{DaSi}}{\varepsilon_{aSi}} - \frac{N_{DcSi}}{\varepsilon_{cSi}}\right) \text{.....(24)}$$

The collection probability profile hence solved for case III using effective lifetime from equation 21.

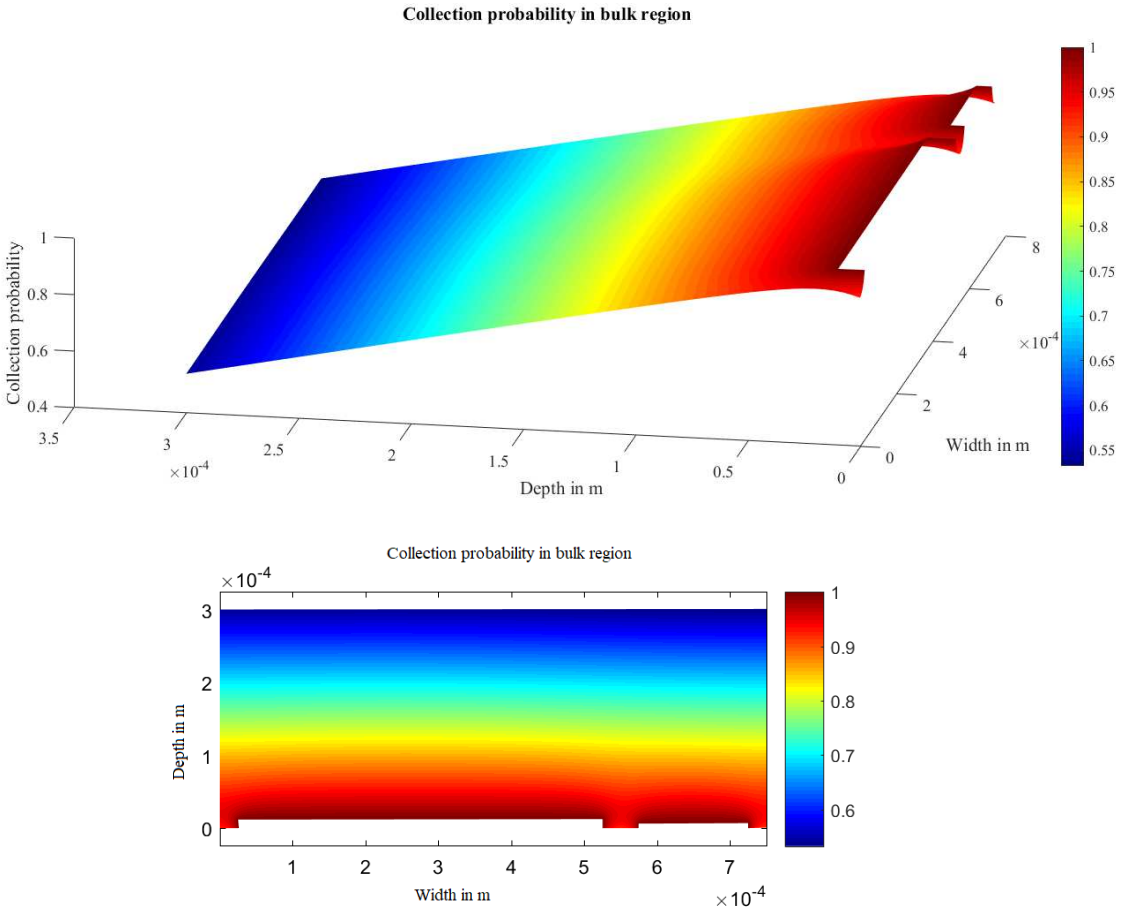

Fig. 12a-12b Collection probability profile in bulk region for Case III

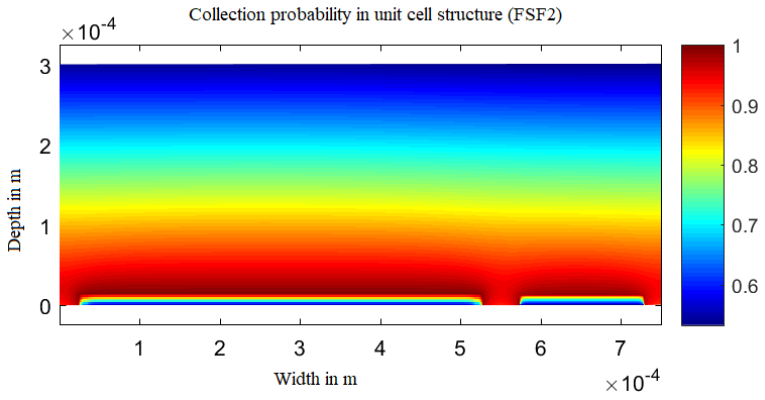

Fig. 13 Collection probability profile in entire unit cell structure for Case III

The estimated current density for FSF of a-Si was 34.09 mA/cm^2.

4. Series and shunt resistance

Series resistance of a solar cell is mainly a contact property. It arises from emitter resistance, BSF resistance and contact resistance in IBC solar cell. The major advantage of IBC is very low value of series resistance. As all the contacts were made at back, almost 86% of the back surface are utilized for metallization.

$$R_s = R_{BSF} + R_e + R_c \text{.....(25)}$$

In equation 22 R_{BSF} and R_e are BSF and emitter finger resistances respectively.

$$R_e = \frac{d_{emitter}}{q\mu_{paSi} N_{AaSi} W_{emitter}} \text{.....(26)}$$

$$R_{BSF} = \frac{d_{BSF}}{q\mu_{naSi} N_{DaSi} W_{BSF}} \text{.....(27)}$$

The contact resistance R_c was considered as a function of carrier concentration as obtained by Schroder et al [19][24].

$$R_c = 10^{(-5\times\log_{10}(N_d)+96.6)} \text{.....(28)}$$

From equation 25 it was evident that R_c is much smaller than R_{BSF} and R_e and hence neglected. Shunt resistance R_{sh} was considered a bulk property and taken as a standard value of 130 Ω [25].

5. Results and discussion

The basic solar cell voltage current relationship was established from the equivalent circuit.

$$I = aJ_L - aJ_0 \exp\left[\frac{q(V_O + IR_S)}{kT}\right] - \frac{V_O + IR_S}{R_{SH}} \text{.....(29)}$$

The V-I characteristics for all three cases of FSF were obtained.

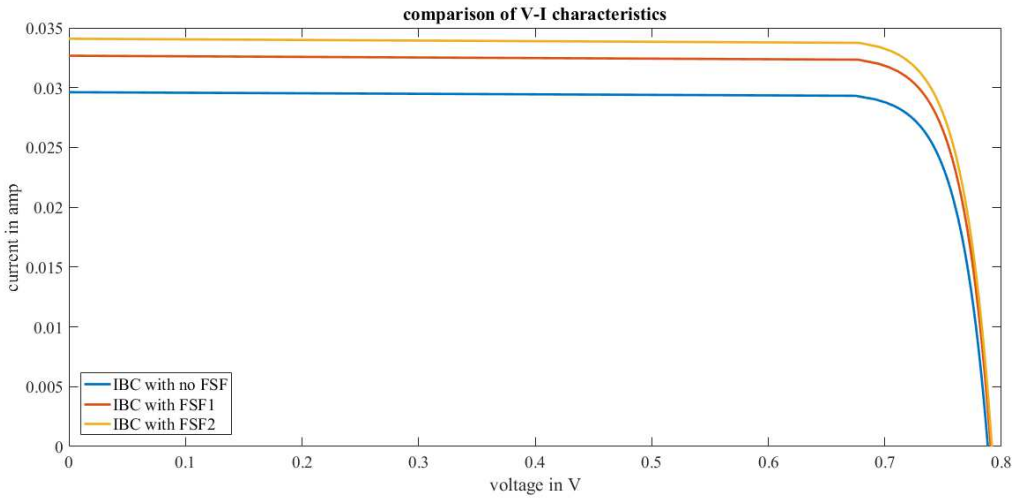

Fig. 14 V-I characteristics of all three FSF IBC solar cells

In Fig. 14 we have shown the V-I characteristics of all three cases of FSF those were modelled. FSF1 was the ZnO film induced FSF while FSF2 was formed by the a-Si:H layer. Different performance parameters were extracted from the V-I characteristics.

Table 2 Performance characteristics of different IBC solar cell

IBC type	V_{OC} in volt	J_{sc} in mA/cm^2	Fill Factor (FF)	% Efficiency (η) (derived from mathematical modelling)	% Efficiency (η) (Experimental/ Simulation published earlier)
No FSF (caseI)	0.8225	28.24	0.8261	19.1887	19.2 [14]
FSF1 (caseII)	0.8263	32.67	0.8265	22.3130	--
FSF2 (caseIII)	0.8274	34.09	0.8267	23.3176	21.5[2]

According to the performance indexes as shown in Table 2 the best result was obtained for FSF2 IBC solar cell. Still the novel SIS FSF1 solar cell is relevant for its lower thermal budget and less complicated fabrication engineering. ZnO film deposition using simple sol-gel techniques are well investigated method [26]. There was a significant improvement in efficiency using the novel SIS FSF modification 19.1887% to 22.3130%.

Further we have investigated the effect of finger area moderation of both BSF and emitter fingers on fill factor and efficiency of IBC with FSF1. We have considered the ratio of area of emitter and BSF to be F_{IBC} and then we varied the ratio to examine the effect on solar cell performance.

$$F_{IBC} = \frac{d_{emitter} W_{emitter}}{d_{BSF} W_{BSF}} \text{.....(30)}$$

F_{IBC} was defined as finger ratio.

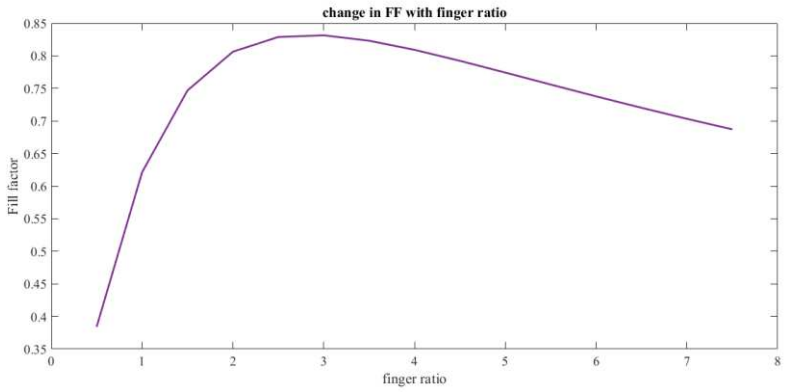

Fig. 15 Variation of fill factor with finger ratio

Fill factor is a contact property. Greater finger ratio indicates lesser BSF area. This resulted greater series resistance and hence there was a drop in fill factor as shown in Fig. 15. Likewise very low finger ratio indicates less emitter area. This was also detrimental for fill factor.

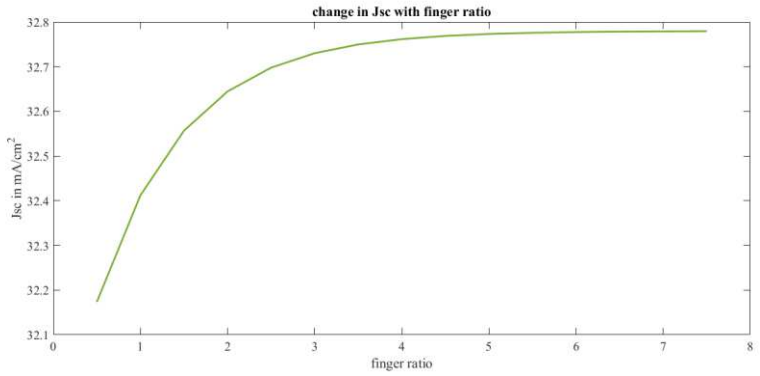

Fig.16 Variation of short circuit current density with finger ratio

Fig. 16 was obtained from simulation varying the finger ratio and computing the corresponding short circuit current density using the method described earlier in this paper. Referring Fig. 6a-6b and Fig. 7a-7b it was clear that the collection probability profile is much better in emitter region than BSF. Thus increasing the finger ratio indicate enhancement of collection probability. This was reflected in Fig. 16 resulting increment of short circuit current density.

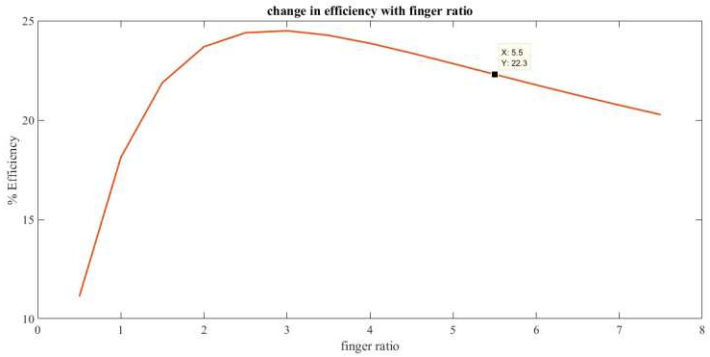

Fig. 17 Variation of efficiency with finger ratio

We have obtained the efficiency vs finger ration graph from change in fill factor and short circuit current with respect to finger ratio. We concluded that increment of finger ratio effects the J_{sc} and FF differently. FF decreased while we have increased the finger ratio but the short circuit current showed the opposite result. Efficiency is a product of FF and J_{sc} . From Fig. 17 it was concluded that the efficiency was maximum at finger ratio ~ 3. Lammert et al predicted the finger ration for maximum efficiency as 2.5[1] with a much lower lifetime.

6. Conclusion

In this paper we have presented a mathematical model of IBC solar cell with a novel FSF technique using ZnO and SiO_2 thin film deposition. The ZnO film can be easily deposited with simple sol-gel method. The SiO_2 can be formed by thermal oxidization. The properties of the ZnO film were taken from experimental reports published earlier. ZnO-SiO_2-C-Si formed a SIS which induced an FSF. We have compared the performance of our proposed IBC structure with existing amorphous Si FSF structure. The simulated results of amorphous Si FSF IBC solar cell were found out to be quite merging with the results published by other scientists [2][3][6]. So we can conveniently conclude this new approach of mathematical modelling has achieved considerable accuracy The MATLAB simulation showed that our SIS FSF enhanced the efficiency of an IBC solar cell without any FSF significantly. But amorphous Si FSF still had better performance. Here we wanted to put our argument that though amorphous Si FSF had better performance than our proposed SIS FSF but SIS FSF fabrication can be done with much less thermal budget and hence the investigation on such SIS structure is still relevant.

Declaration

Funding: No institutional funding was used

Conflicts of interest/Competing interests: Not any

Availability of data and material: Available with authors.

Code availability: Available with authors.

Authors' contributions:

Kaustuv Dasgupta: Writing the manuscript, Theoretical analysis, Coding, Result Analysis

Utpal Gangopadhyay: Ideation, Supervising, Data analysis

Anup Mondal: Supervising, data correction

Soma Ray: Technical support, Data analysis

Compliance with ethical standards: The study was not funded by any funding organization. MATLAB software used in the study is licensed under Meghnad Saha Institute of Technology. The authors declare that they have no conflicts of interest. This article does not contain any studies involving animals performed by any of the authors. This article does not contain any studies involving human participants performed by any of the authors.

Consent to participate: This article does not contain any studies involving human participants performed by any of the authors.

Consent for Publication: We give our consent for the publication of identifiable details, which can include photograph(s) and/or videos and/or case history and/or details within the text ("Material") to be published in the Silicon, Springer. Therefore, anyone can read material published in the Journal.

Acknowledgments: We acknowledge Meghnad Saha Institute of Technology for providing us with MATLAB software for simulation.

References

[1] R. J. Schwartz and M. D. Lammert, "Silicon solar cells for high concentration applications," 1975 International Electron Devices Meeting, Washigton, DC, USA, 1975, pp. 350-352.

[2] Diouf, D.; Kleider, J.; Desrues, T. & Ribeyron, P.-J., Effects of the front surface field in n-type interdigitated back contact silicon heterojunctions solar cells, Energy Procedia, 2010, 2, 59-64

[3] Bao, J.; Liu, A.; Lin, Y. & Zhou, Y., An insight into effect of front surface field on the performance of interdigitated back contact silicon heterojunction solar cells, Materials Chemistry and Physics, 2020, 255, 123625

[4] M. D. Lammert and R. J. Schwartz, "The interdigitated back contact solar cell: A silicon solar cell for use in concentrated sunlight," in IEEE Transactions on Electron Devices, vol. 24, no. 4, pp. 337-342, April 1977

[5] Kim, S. M.; Chun, S.; Kang, M. G.; Song, H.-E.; Lee, J.-H.; Boo, H.; Bae, S.; Kang, Y.; Lee, H.-S. & Kim, D., Simulation of interdigitated back contact solar cell with trench structure , Journal of Applied Physics, 2015, 117, 074503

[6] Diouf, D.; Kleider, J.; Desrues, T. & Ribeyron, P.-J., Study of interdigitated back contact silicon heterojunctions solar cells by two-dimensional numerical simulations, Materials Science and Engineering: B, 2009, 159-160, 291-294

[7] R. Ghosh, G.K. Paul, D. Basak, Effect of thermal annealing treatment on structural, electrical and optical properties of transparent sol–gel ZnO thin films, Materials Research Bulletin, Volume 40, Issue 11, 2005, Pages 1905-1914

[8] Hussain, B.; Aslam, A.; Khan, T.M.; Creighton, M.; Zohuri, B. Electron Affinity and Bandgap Optimization of Zinc Oxide for Improved Performance of ZnO/Si Heterojunction Solar Cell Using PC1D Simulations. Electronics 2019, 8, 238

[9] D.P. Norton, Y.W. Heo, M.P. Ivill, K. Ip, S.J. Pearton, M.F. Chisholm, T. Steiner, ZnO: growth, doping & processing, Materials Today, Volume 7, Issue 6, 2004

[10] Ondo-Ndong, R., Essone-Obame, H., Moussambi, Z.H. et al. Capacitive properties of zinc oxide thin films by radiofrequency magnetron sputtering. J Theor Appl Phys 12, 309–317

[11] Liehr, M.; Lewis, J. E. & Rubloff, G. W., Kinetics of high-temperature thermal decomposition of SiO2 on Si(100) , Journal of Vacuum Science & Technology A, 1987, 5, 1559-1562

[12] Nichiporuk, O.; Kaminski, A.; Lemiti, M.; Fave, A. & Skryshevsky, V., Optimisation of interdigitated back contacts solar cells by two-dimensional numerical simulation, Solar Energy Materials and Solar Cells, 2005, 86, 517-526

[13] Fahrner**.** Wolfgang Rainer (Ed.), Amorphous Silicon / Crystalline Silicon Heterojunction Solar Cells, Springer Briefs in Applied Sciences and Technology, Springer-Verlag Berlin Heidelberg , 2013, p -13

[14] Bateman, N.; Sullivan, P.; Reichel, C.; Benick, J. & Hermle, M., High quality ion implanted boron emitters in an interdigitated back contact solar cell with 20% efficiency, Energy Procedia, 2011, 8, 509-514

[15] Schaper, M., Schmidt, J., Plagwitz, H. and Brendel, R. (2005), 20.1%-efficient crystalline silicon solar cell with amorphous silicon rear-surface passivation. Prog. Photovolt: Res. Appl., 13: 381-386.

[16] McIntosh, Keith & Honsberg, C.. (2000). The Influence of Edge Recombination on a Solar Cell's Iv Curve.

[17] Richard S. Muller, Theodore I. Kamins, Device Electronics for Integrated Circuits, 3rd Edition, October 2002

[18] Markvart T, Castañer L, Chapter IA-2 Semiconductor Materials and Modelling in Practical Handbook of Photovoltaics , p. 95-121, Elsevier Science, 2003.

[19] Kaustuv Dasgupta, Soma Ray, Anup Mondal, Utpal Gangopadhyay, Review on different front surface modification of both n+-p-p+ and p+-n-n+ C- Si solar cell, Materials Today: Proceedings, Volume 4, Issue 14, 2017, Pages 12698-12707

[20] Green, M.A. and Keevers, M.J. (1995), Optical properties of intrinsic silicon at 300 K. Prog. Photovolt: Res. Appl., 3: 189-192.

[21] Donolato, C., A reciprocity theorem for charge collection, Applied Physics Letters, 1985, 46, 270-272

[22] Donolato, C., Reciprocity theorem for charge collection by a surface with finite collection velocity: Application to grain boundaries , Journal of Applied Physics, 1994, 76, 959-966

[23] Richard S. Muller, Theodore I. Kamins, Device Electronics for Integrated Circuits, 3rd Edition, October 2002

[24] Schroder DK, Meier DL, Solar cell contact resistance—A review, IEEE Transactions on Electron Devices, 1984, vol. 31, no. 5, p. 637-647.

[25] S. Roy and R. Gupta, "Quantitative Estimation of Shunt Resistance in Crystalline Silicon Photovoltaic Modules by Electroluminescence Imaging," in IEEE Journal of Photovoltaics, vol. 9, no. 6, pp. 1741-1747

[26] Lamia Znaidi, Sol–gel-deposited ZnO thin films: A review, Materials Science and Engineering: B,

Volume 174, Issues 1–3, 2010, Pages 18-30.

Figures

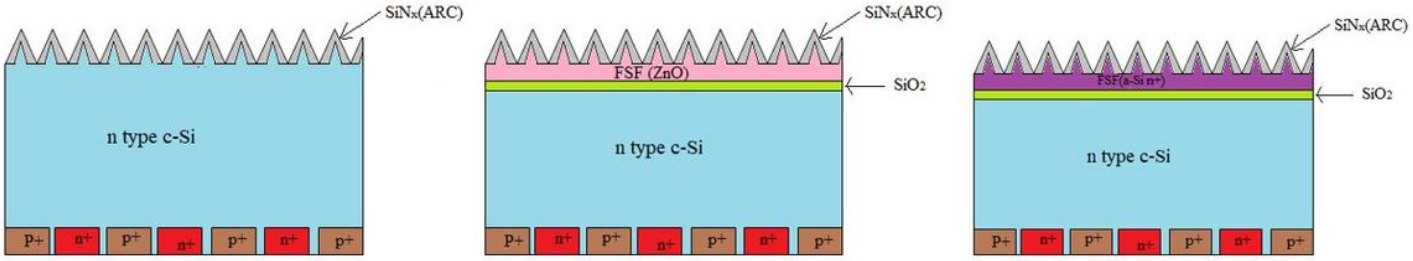

Figure 1

1a -1c Structure of interdigitated back contact solar cell with and without FSF

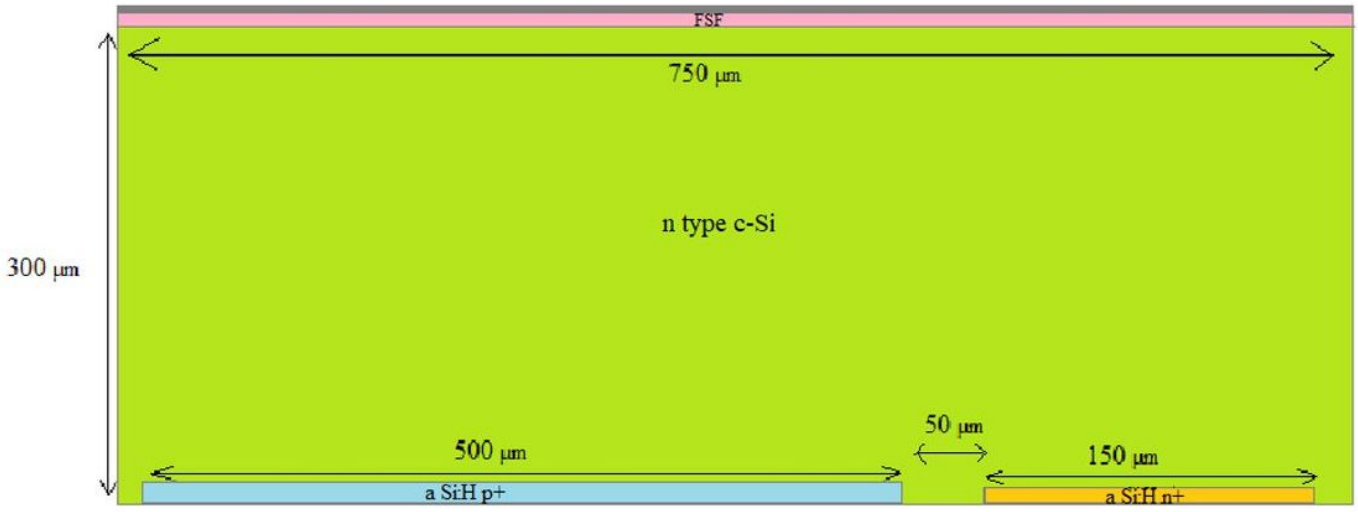

Figure 2

Unit Cell Structure

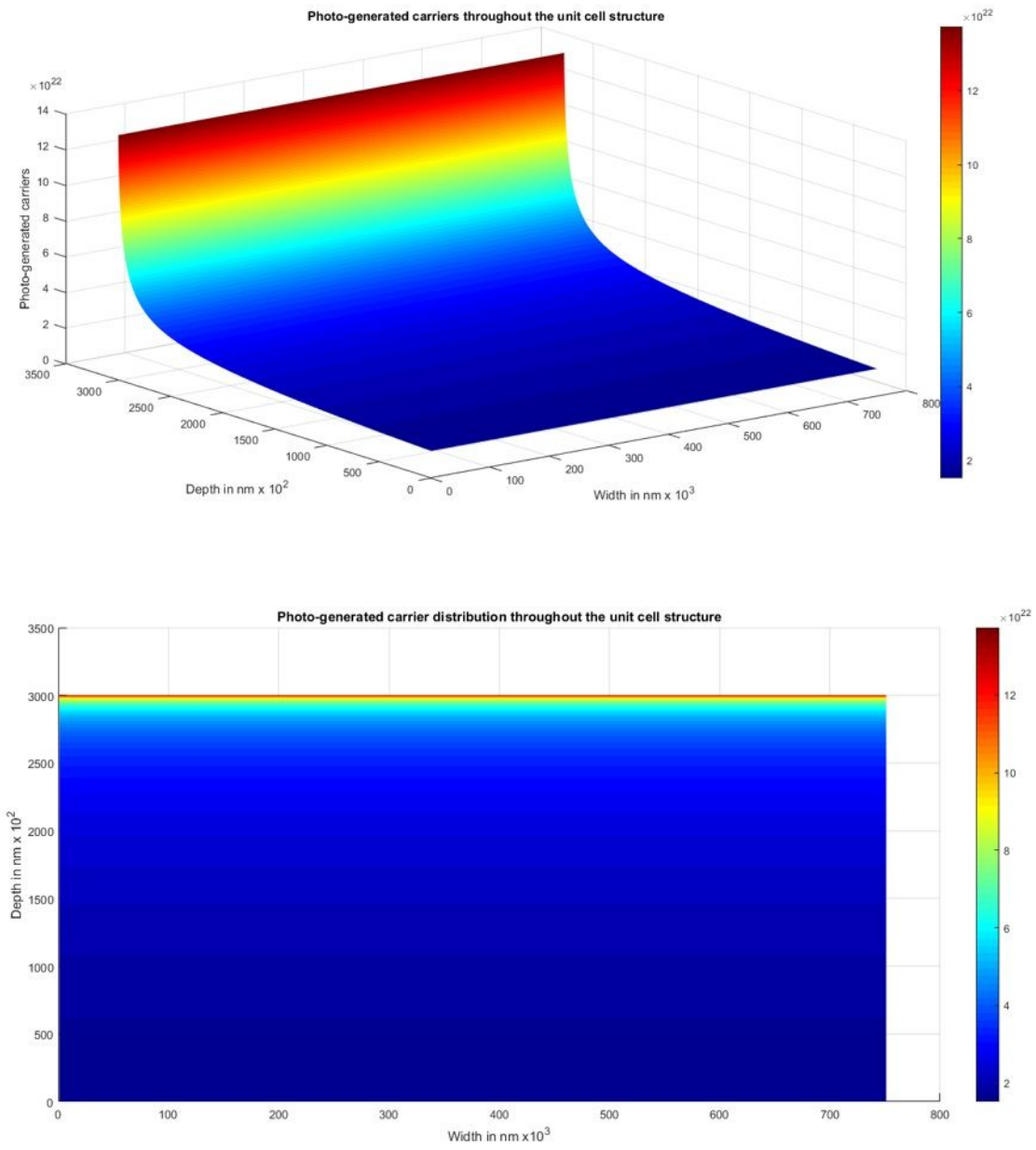

Figure 3

3a-3b Photo-generated carrier distribution throughout unit cell structure

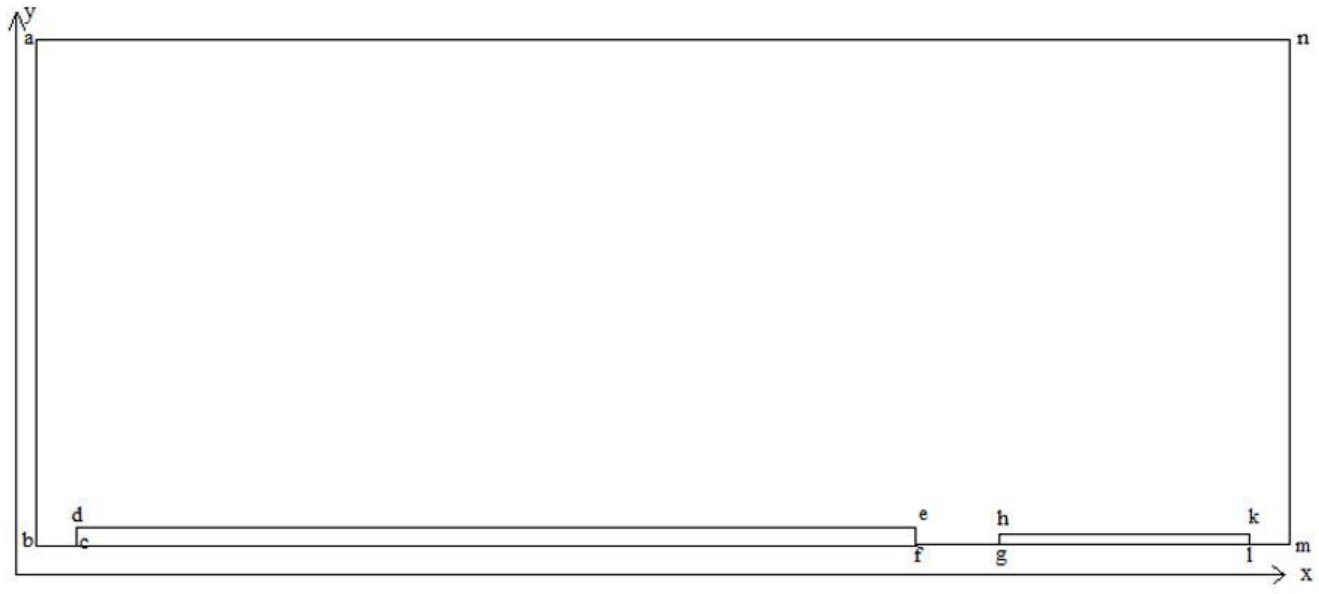

Figure 4

Boundaries of unit cell structure

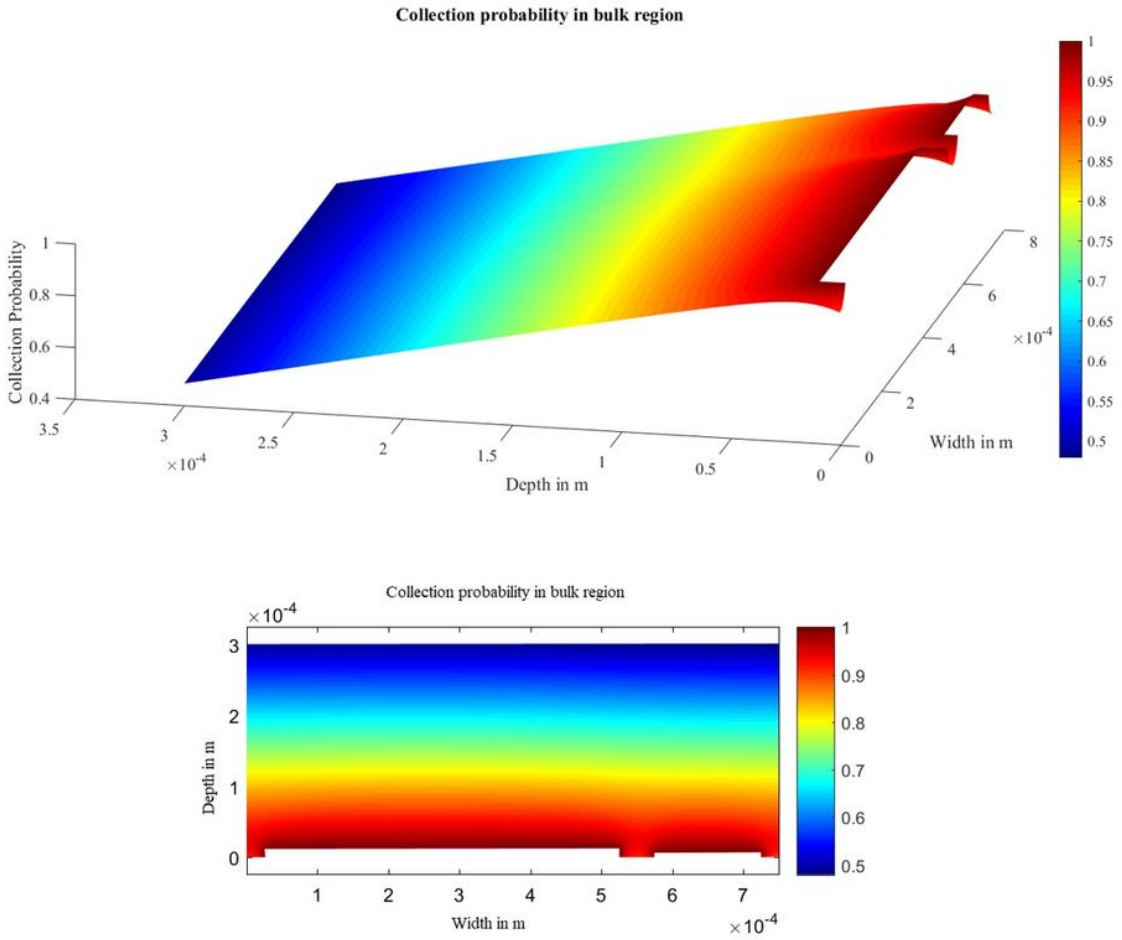

Figure 5

a-5b Collection probability profile in bulk region for Case I

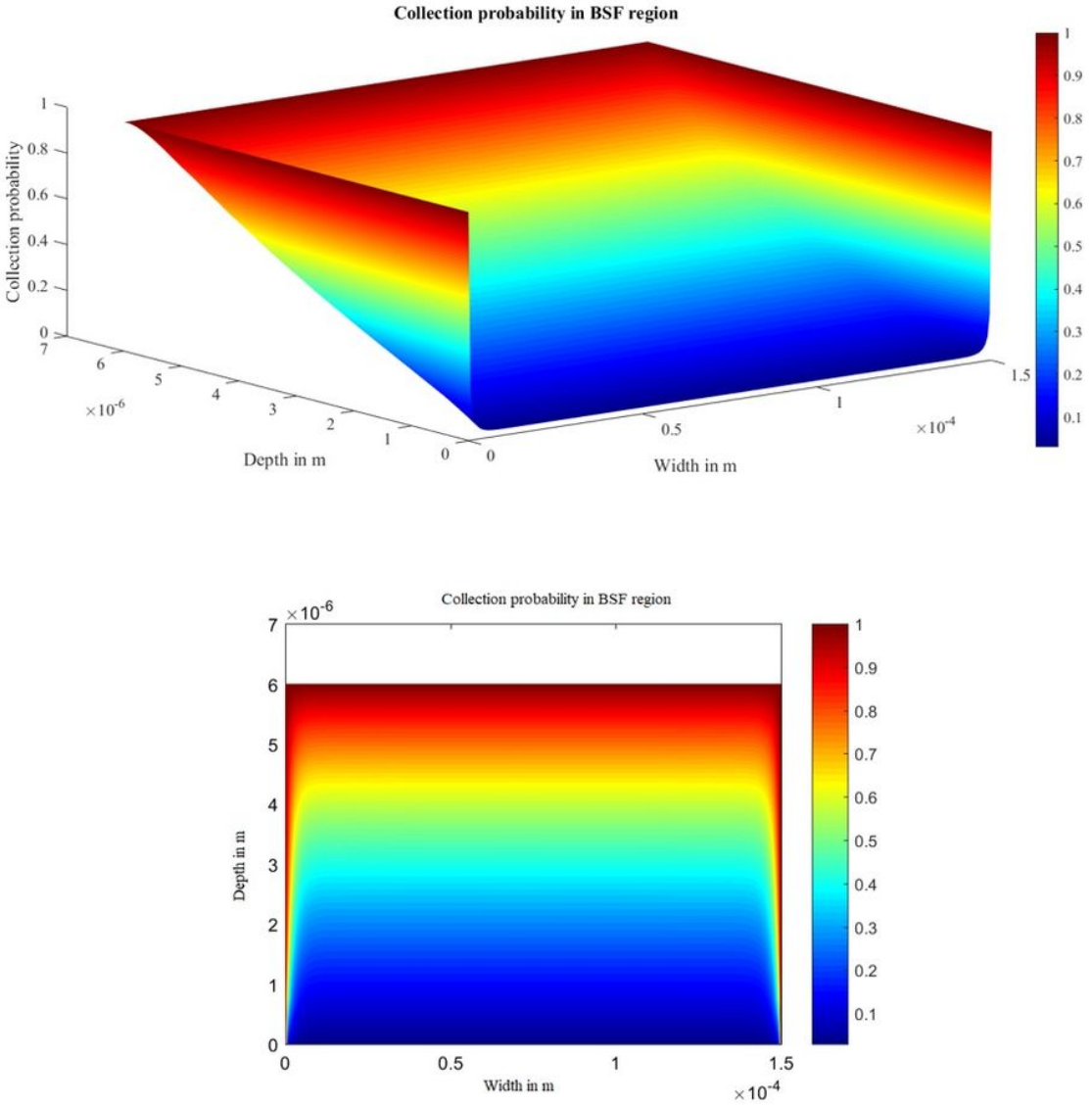

Figure 6

6a-6b Collection probability profile in emitter region

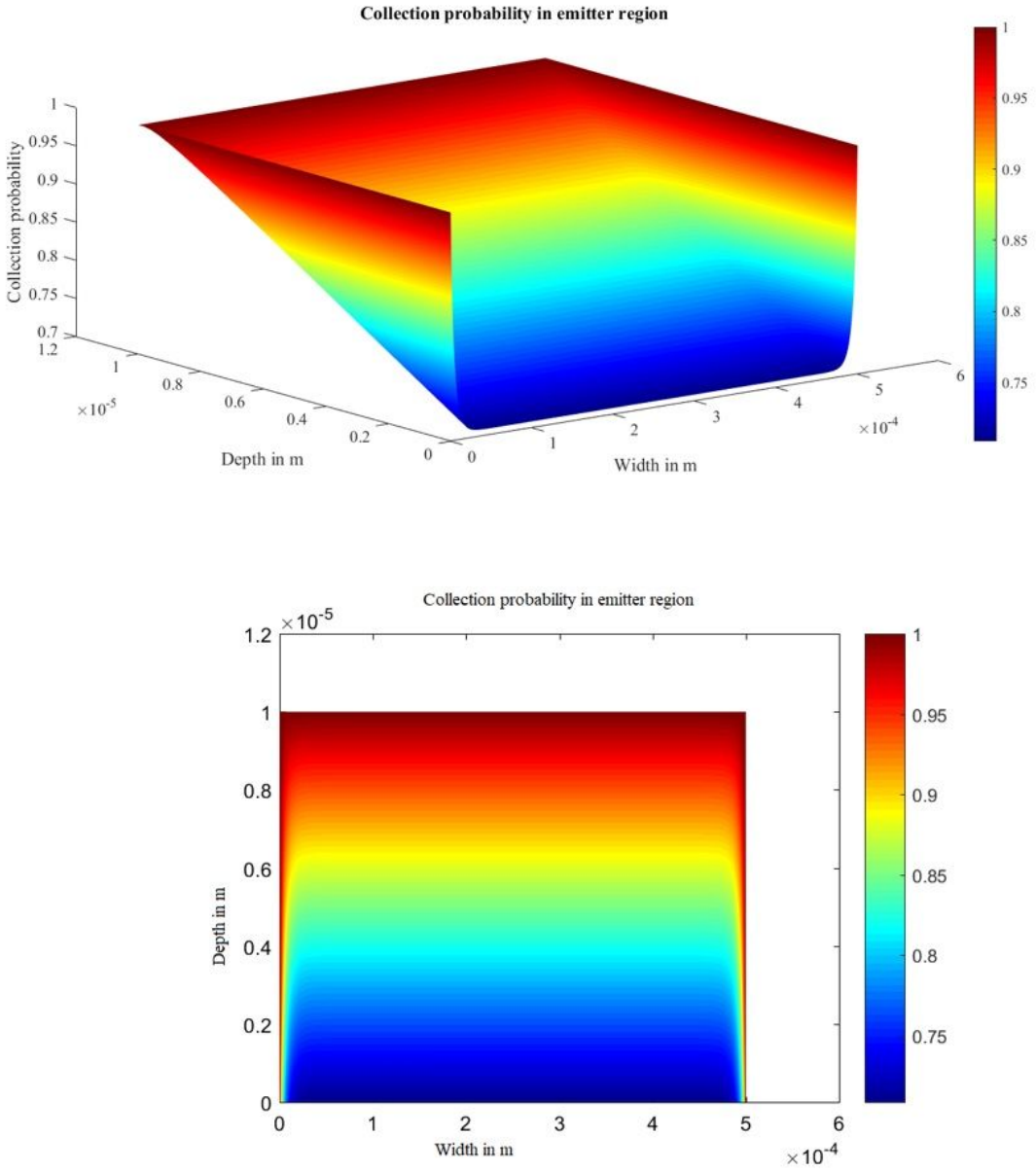

Figure 7

7a-7b Collection probability profile in emitter region

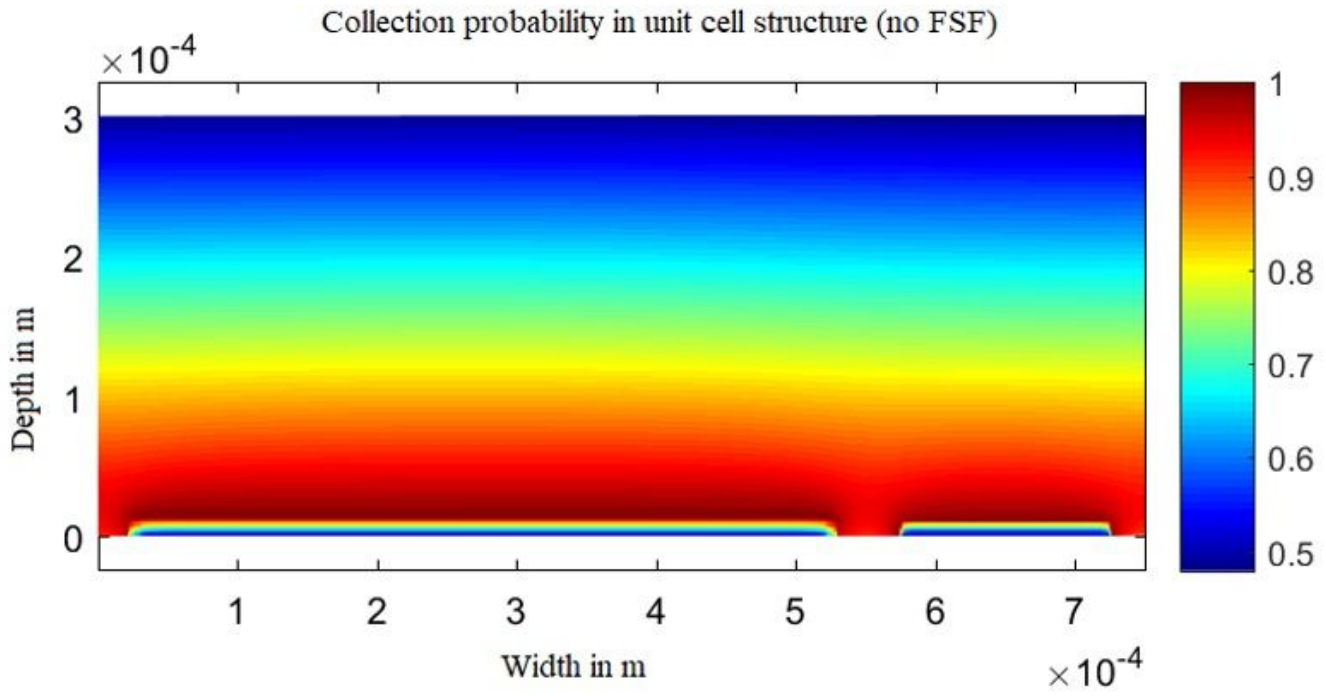

Figure 8

Collection probability profile in entire unit cell structure for Case I

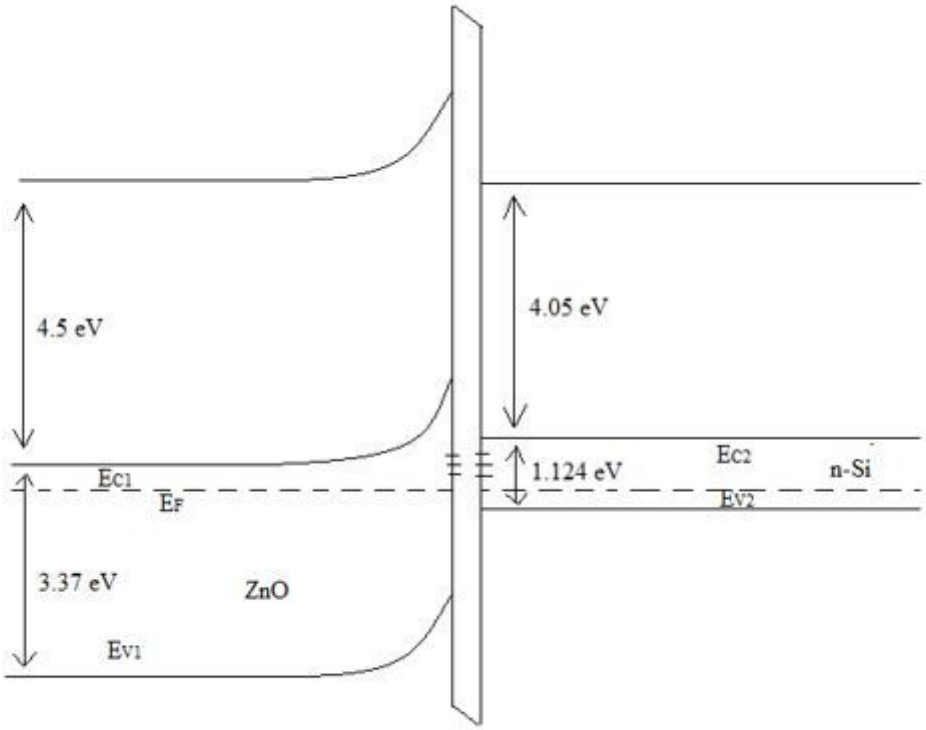

Figure 9

Energy band diagram of FSF SIS junction

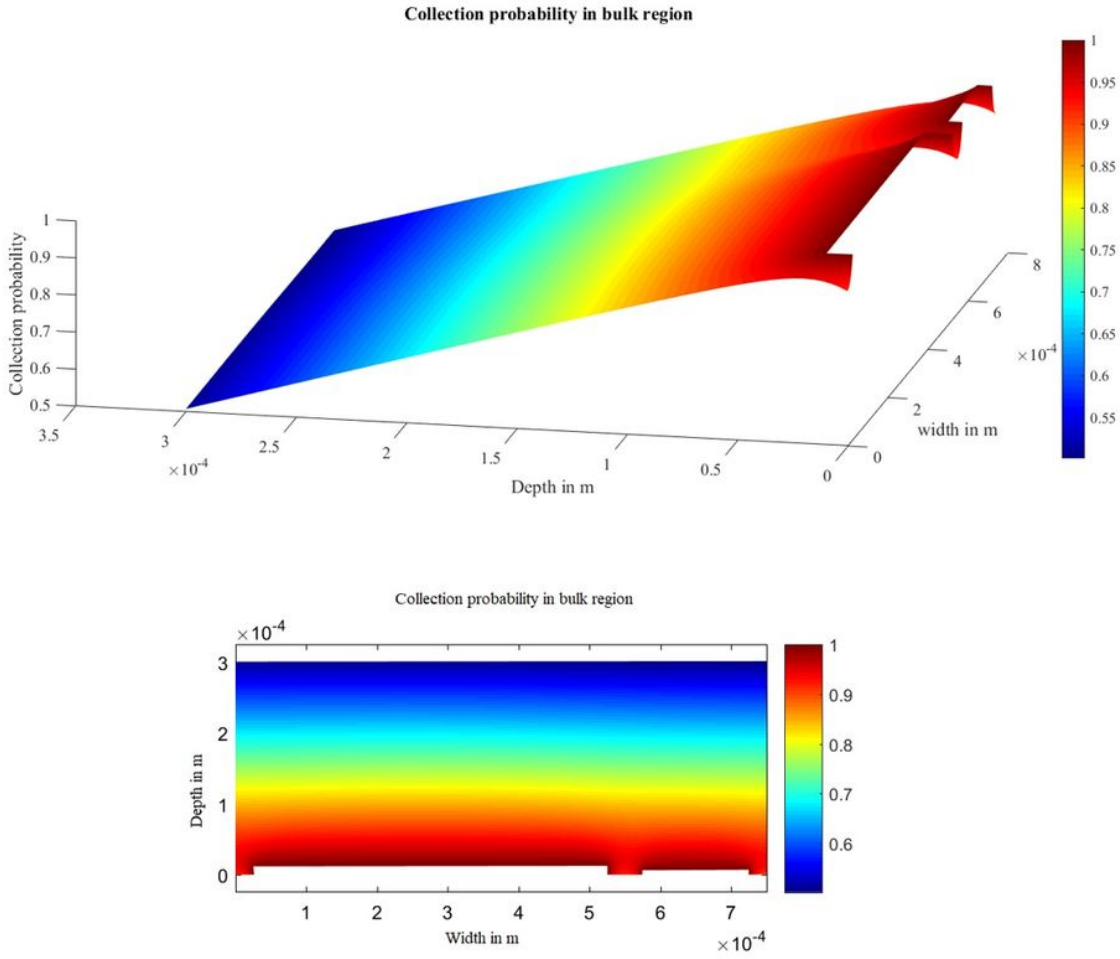

Figure 10

10a-10b Collection probability profile in bulk region for Case II

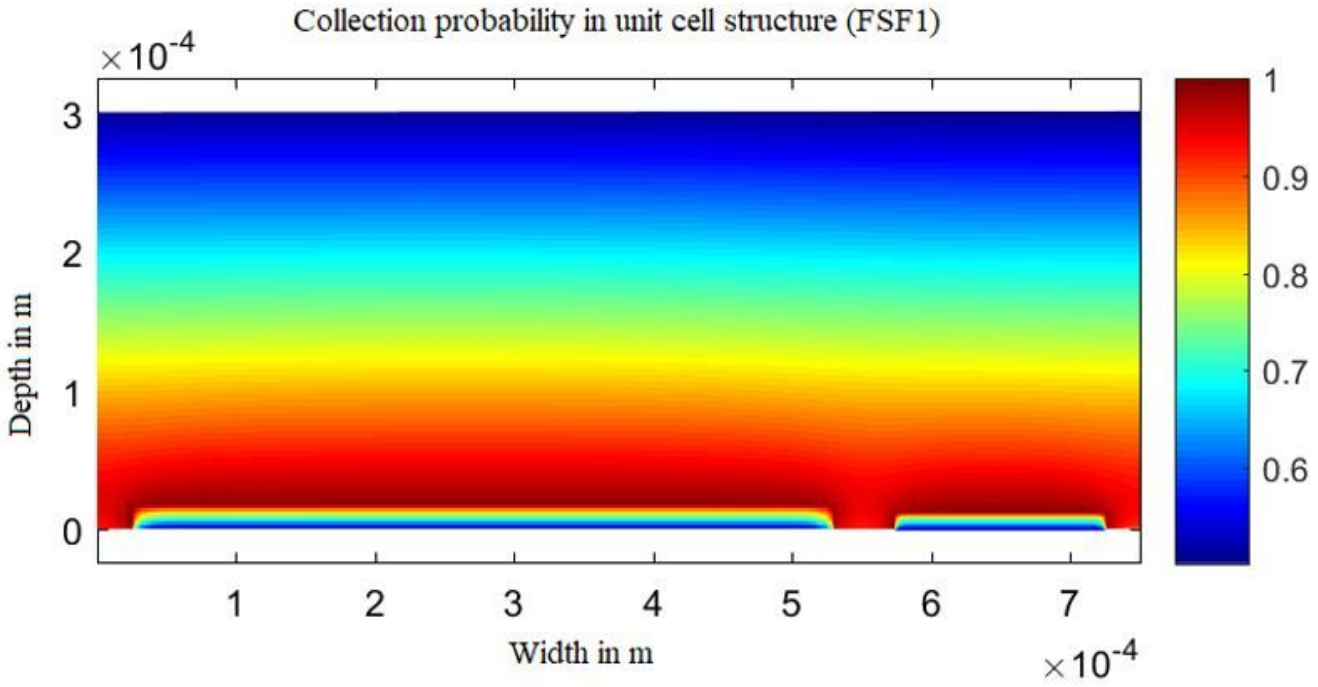

Figure 11

Collection probability profile in entire unit cell structure for Case II

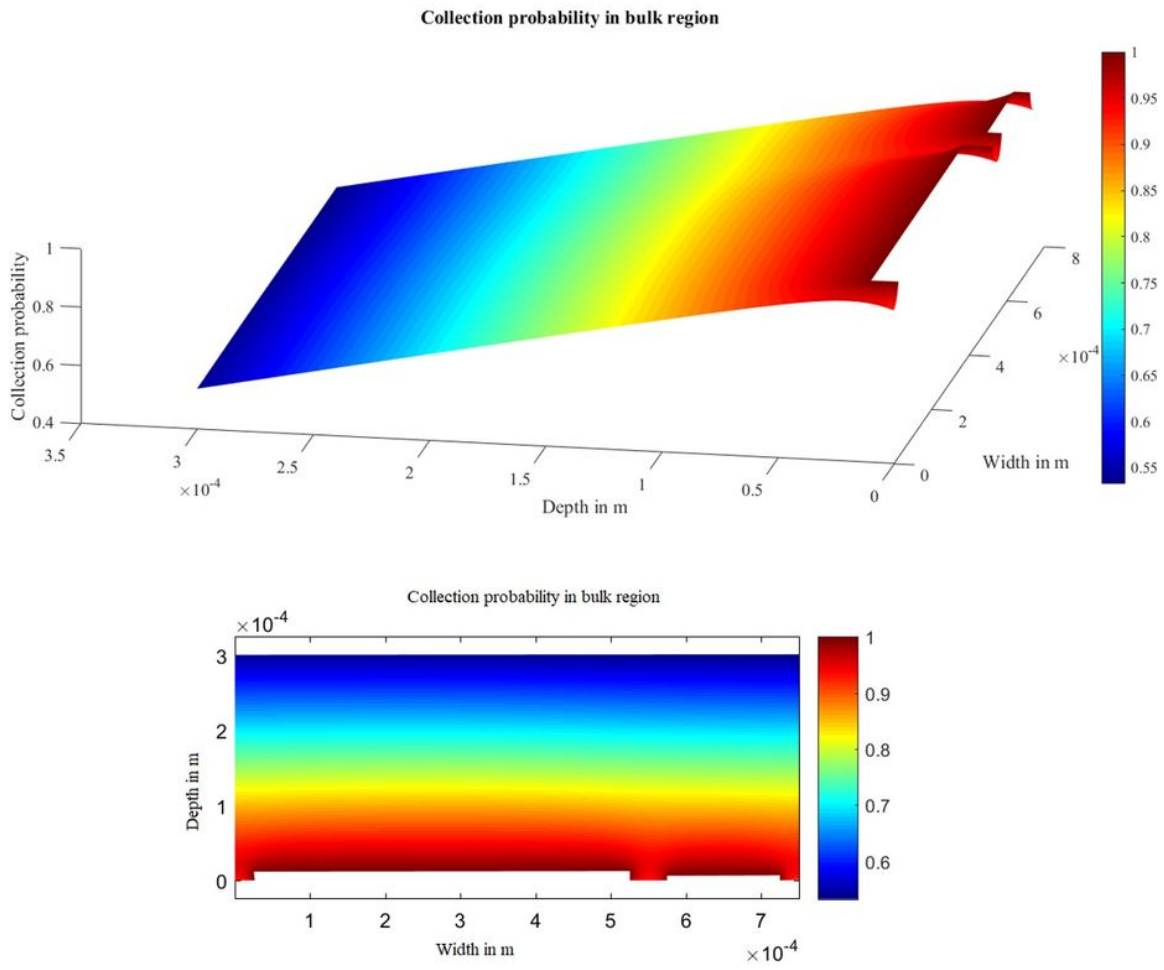

Figure 12

12a-12b Collection probability profile in bulk region for Case III

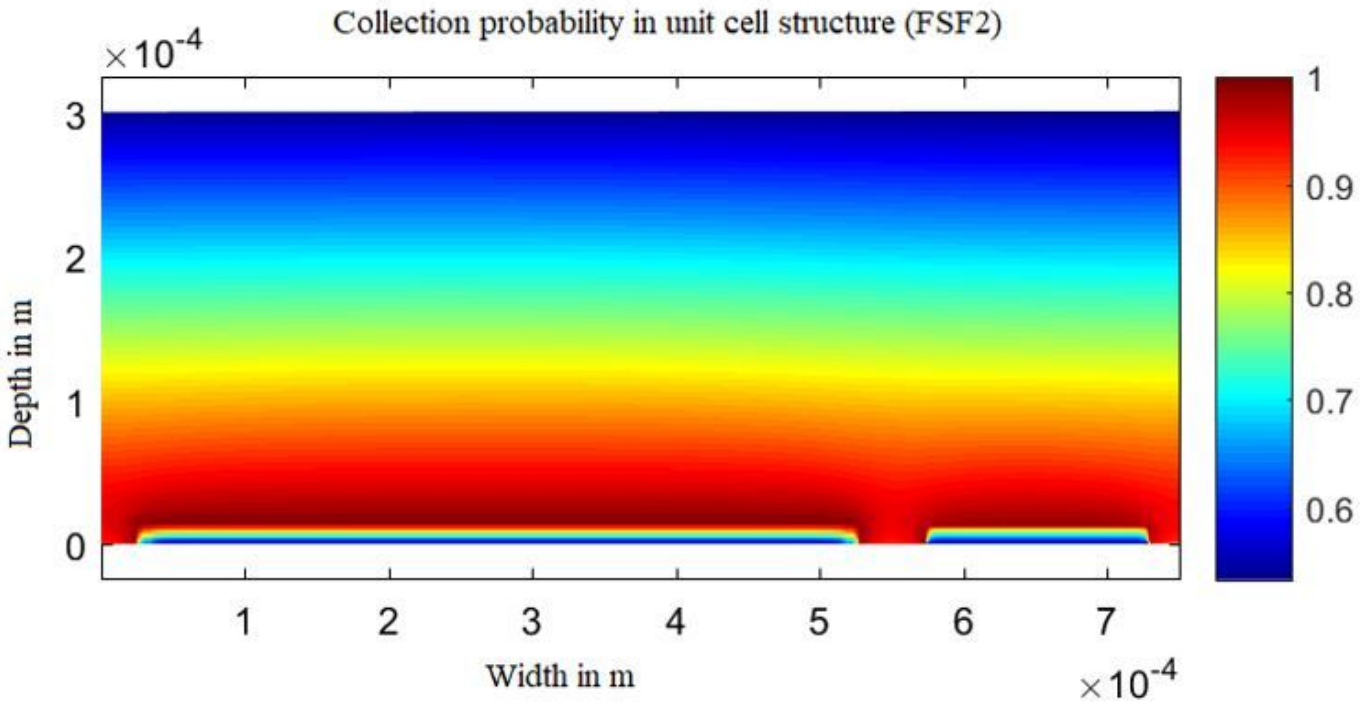

Figure 13

Collection probability profile in entire unit cell structure for Case III

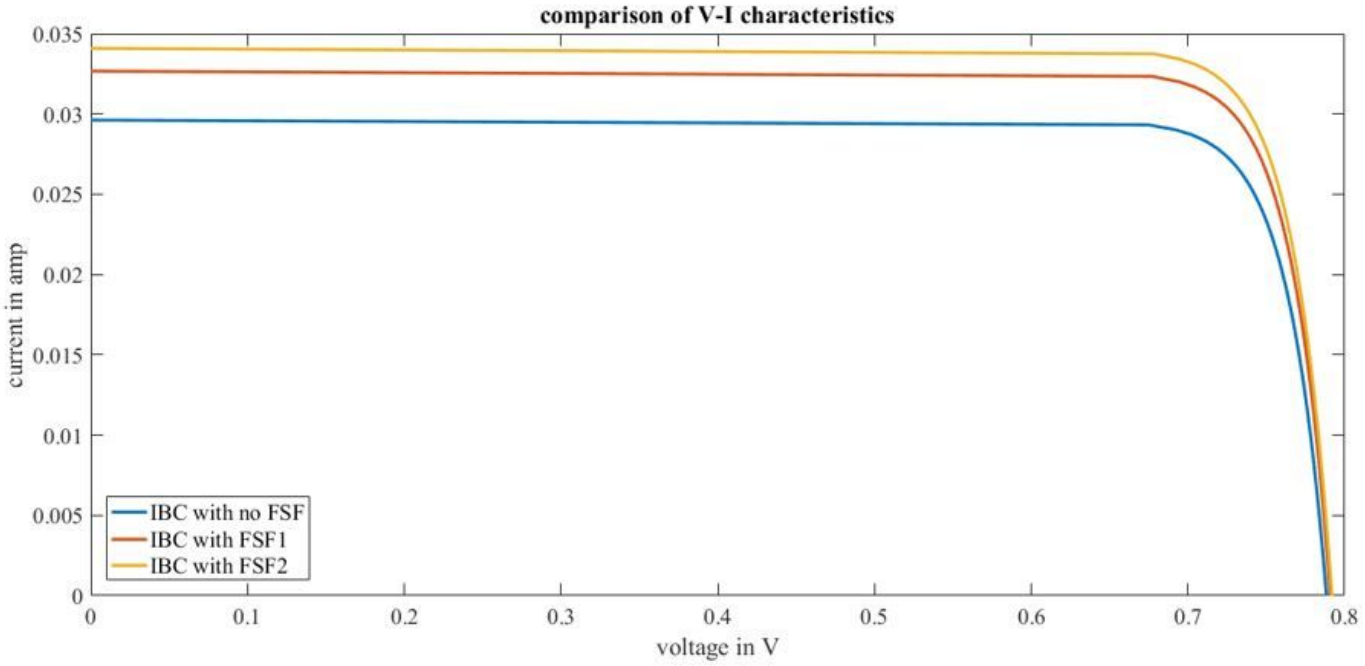

Figure 14

V-I characteristics of all three FSF IBC solar cells

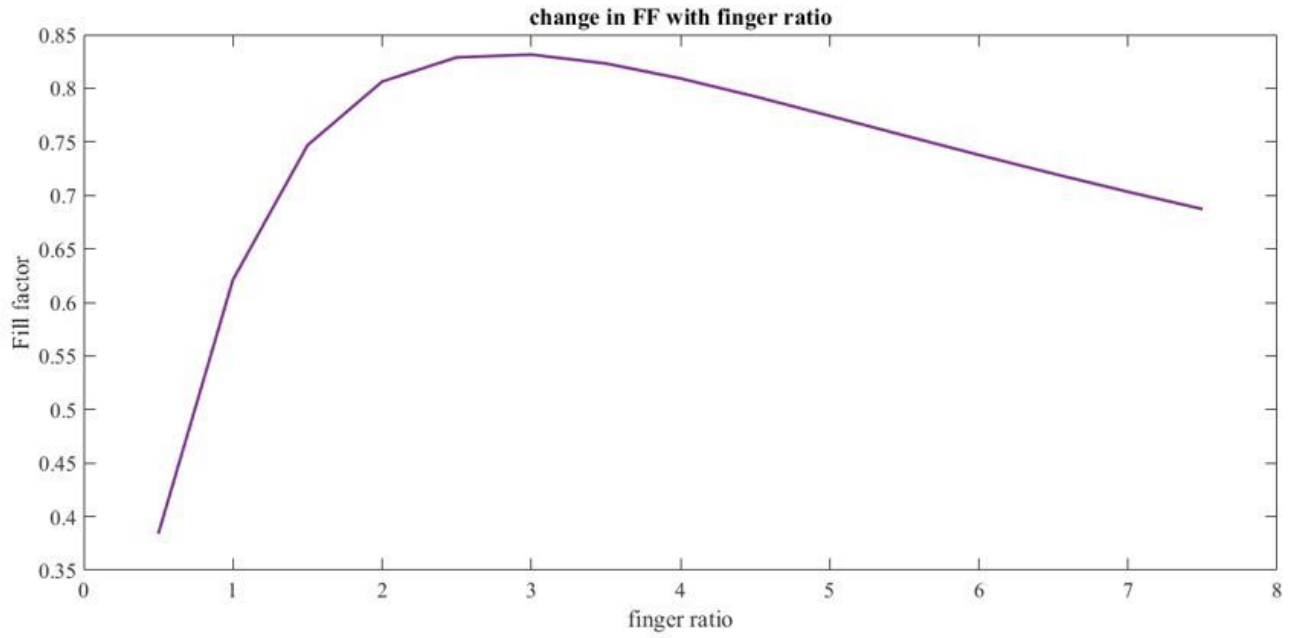

Figure 15

Variation of fill factor with finger ratio

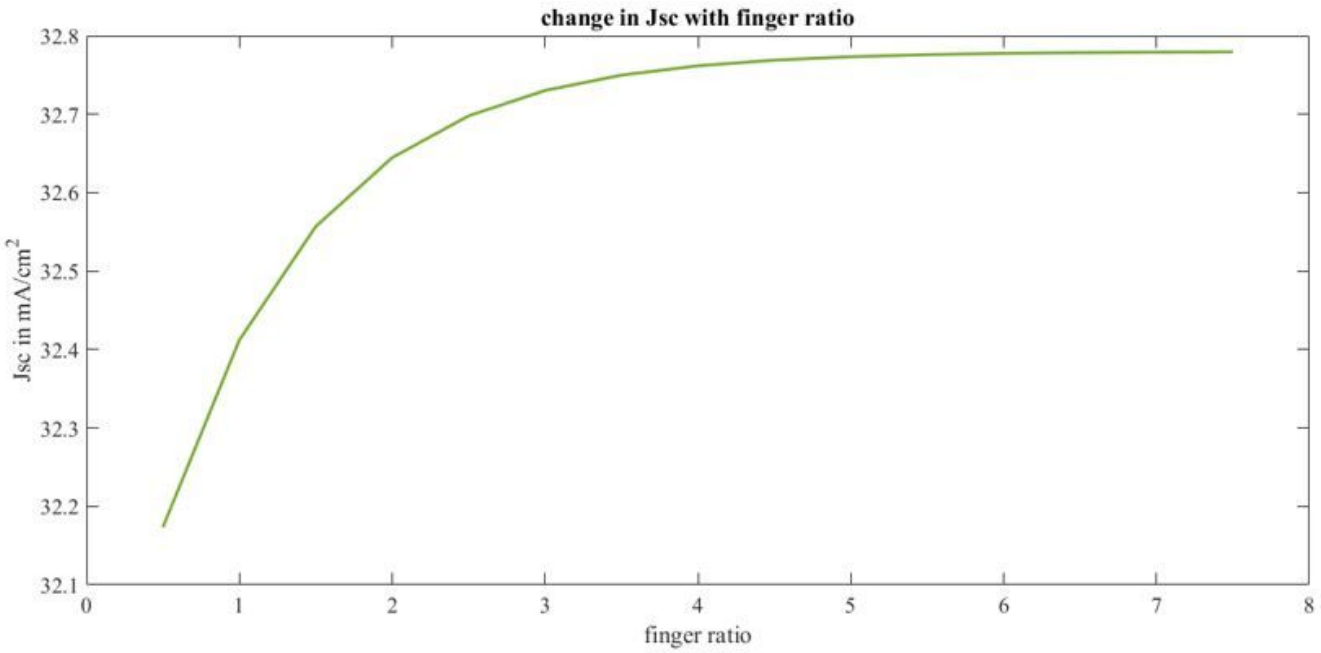

Figure 16

Variation of short circuit current density with finger ratio

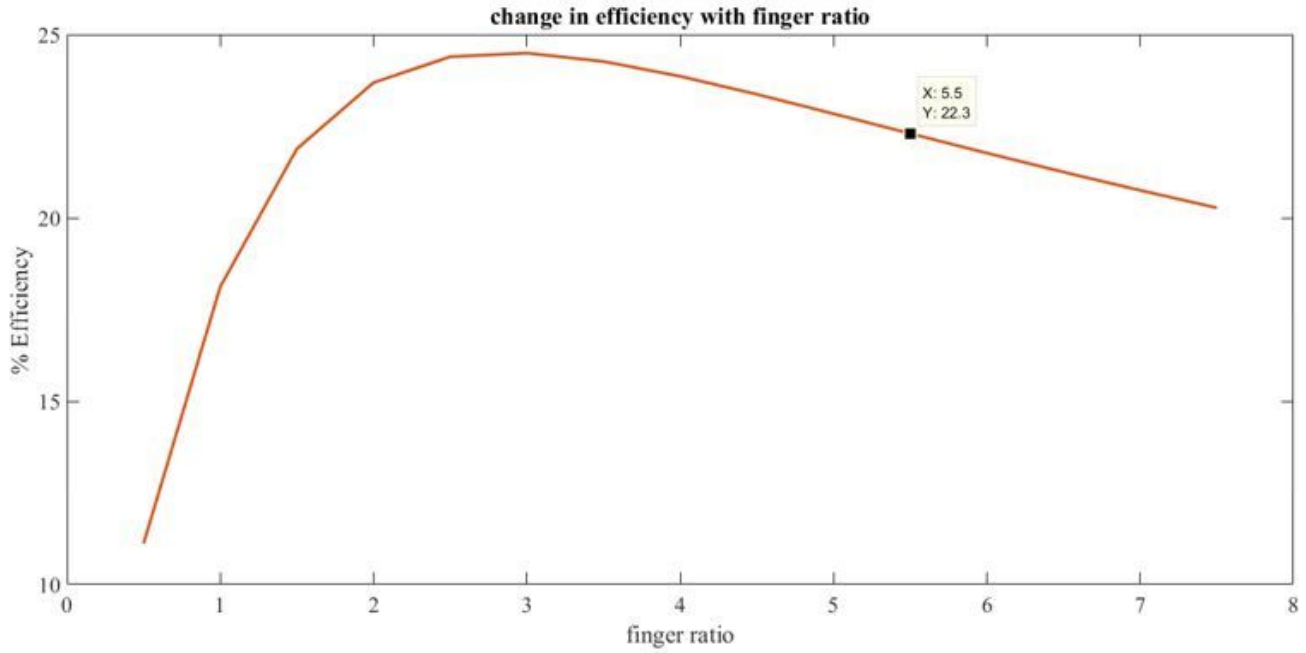

Figure 17

Variation of efficiency with finger ratio